57-7-55

NATIONAL ADVISORY COMMITTEE FOR AERONAUTICS

TECHNICAL NOTE 4130

NACA 65-SERIES COMPRESSOR ROTOR PERFORMANCE WITH VARYING ANNULUS-AREA RATIO, SOLIDITY, BLADE ANGLE, AND REYNOLDS NUMBER AND COMPARISON WITH CASCADE RESULTS

By Wallace M. Schulze, John R. Erwin,
and George C. Ashby, Jr.

Langley Aeronautical Laboratory
Langley Field, Va.

Washington

October 1957

NATIONAL ADVISORY COMMITTEE FOR AERONAUTIC

TECHNICAL NOTE 4130

NACA 65-SERIES COMPRESSOR ROTOR PERFORMANCE WITH VARYING ANNULUS-AREA RATIO, SOLIDITY, BLADE ANGLE, AND REYNOLDS NUMBER AND COMPARISON WITH CASCADE RESULTS[1]

By Wallace M. Schulze, John R. Erwin,
and George C. Ashby, Jr.

SUMMARY

A typical axial-flow compressor rotor using NACA 65-series compressor blades was tested at low speeds and its performance was measured over a range of quantity flow rates at several values of annulus-area ratio, blade-setting angle, solidity, and Reynolds number to compare with porous-wall cascade results. The data obtained with the annulus area varied were corrected to the two-dimensional-flow condition by two methods. From the results of this study, the conclusion was reached that two-dimensional-flow porous-wall cascade results can be used to estimate rotor performance with good accuracy over a wide range of conditions. The mean-axial-velocity method of converting the rotor data to two-dimensional-flow conditions gave good agreement with cascade data for axial-velocity changes across the rotor as large as 15 percent. The rotor performance changed only slightly as the Reynolds number was decreased from 500,000 to 250,000. As the Reynolds number was decreased below 250,000, decreases in rotor efficiency, pressure-rise coefficient, and turning angle were observed.

INTRODUCTION

The performance of axial-flow compressor blades can be quickly and accurately measured in detail by using stationary models in two-dimensional-flow cascade wind tunnels. The cascade tunnel can thus be a very useful instrument for providing information needed in the design of axial-flow compressors. Questions often arise as to whether two-dimensional-flow cascade data can be applied directly to compressors and what corrections, if any, must be made. In the investigation reported in reference 1,

[1]Supersedes declassified NACA Research Memorandum L52L17 by Wallace M. Schulze, John R. Erwin, and George C. Ashby, Jr.

rotor-blade surface pressure distributions and air-turning-angle values were found to be similar to those measured in porous-wall cascade tests at design angle of attack. The present investigation was devised to provide information concerning the effect on rotor efficiency, static-pressure and total-pressure rise, and turning angle of changes in blade angle, solidity, flow rate, Reynolds number, and annulus area through the rotor. The performance of the rotor as estimated from cascade data was calculated and is presented for comparison.

An axial-flow compressor rotor having blades of camber, solidity, and hub-tip radius ratio typical of a centrally located rotor in a multi-stage compressor was investigated at low speed in a 28-inch test compressor without guide vanes or stators. Surveys of the flow made immediately upstream and downstream of the rotor were used in calculating the performance for comparison with values estimated from porous-wall-cascade test results.

SYMBOLS

A	annulus area, sq ft
c_d	section drag coefficient
c_l	section lift coefficient
L/D	lift-drag ratio
D	diameter, ft
E	energy added to air as total pressure, ft-lb/sec
I	work done on air by rotor, ft-lb/sec
M	mass flow, slugs/sec
n	rotor speed, rps
p_s	static pressure, lb/ft^2
P_T	total pressure, lb/ft^2
Q	quantity flow of air, ft^3/sec
q	dynamic pressure, lb/ft^2

R	Reynolds number based on blade chord length, entering velocity and standard stagnation density and viscosity
r	radius, ft
U	rotor blade velocity, ft/sec (except in fig. 1 where U is expressed as a fraction of the blade tip velocity)
V	airspeed respective to stationary casing, ft/sec (except in fig. 1 where V is expressed as a fraction of the blade tip velocity)
W	airspeed respective to rotor, ft/sec (except in fig. 1 where W is expressed as a fraction of the blade tip velocity)
α	angle of attack relative to blade chord, deg
β	inlet and outlet air angle relative to blades, deg from axis
δ	ratio of tangential velocity change through the rotor to entering axial velocity
γ	ratio of specific heats
ξ	blade-angle setting respective to rotor axis, deg
η	adiabatic efficiency, percent
θ	air turning angle, deg
ρ	air density, slugs/ft^3
σ	solidity, blade chord divided by blade gap
φ	air angle in stationary coordinates, deg from axis
Φ	quantity coefficient, $\frac{Q}{nD_t^3}$
ψ_s	static-pressure-rise coefficient, $\frac{p_{s_2} - p_{s_1}}{\frac{1}{2}\rho U_t^2}$
ψ_T	total-pressure-rise coefficient, $\frac{P_{T_2} - P_{T_1}}{\frac{1}{2}\rho U_t^2}$

Subscripts:

1	upstream of blade row
2	downstream of blade row
a	axial direction
d	design condition
e	value based on vector diagram corrected to mean axial velocity
f	value based on vector diagram corrected to entering axial velocity
h	at hub section, $D/D_t = 0.784$
p	at pitch section, $D/D_t = 0.892$
t	at tip section, $D/D_t = 1.000$
tan	tangential component
ch	settling chamber

APPARATUS AND TESTS

Apparatus.- A schematic diagram of the test compressor is presented in figure 2. The flow enters from the atmosphere through three screens into the settling chamber. An entrance cone having a contraction ratio of 13:1 is used to accelerate the flow into the test section. The rotor discharges through an annular diffuser equivalent to 6° conical expansion. At the end of the annular diffuser, the flow is turned outward through a radial diffuser which can be adjusted to decrease or increase the exit area and thus regulate the flow rate. The drive is a 75-horsepower direct-current motor operable from 0 to 3,600 rpm.

The annular test section has an inner-casing diameter of 21.82 inches and an outer-casing diameter of 27.82 inches; the hub-tip radius ratio is 0.784. The tests were made on the $\delta = 0.6$ blades originally reported in reference 2. Porous-wall cascade design data from reference 3

indicated that the design conditions should be changed slightly from the original values of reference 2, see table I. The design is free vortex using NACA 65-series airfoil sections cambered for isolated airfoil lift coefficients of 1.2, 1.1, and 1.0 at the 30-percent (inboard section), 50-percent (pitch section), and 70-percent (outboard section) annulus height positions, respectively. The blades have a constant chord and height of 3 inches. The solidity was varied by changing the number of blades. For the pitch-section solidities of 1.0 and 0.5, the number of blades used was 26 and 13, respectively. The average tip clearance was approximately 0.015 inch or 1/2 percent of blade height. A rotating inner casing extending 5 inches beyond the blades was attached to the rotor to support the rotor-mounted instruments and the balsa fairings used to vary the annulus area (fig. 3). All three annulus-area changes were made by altering the inner-casing diameter for a short distance along the test section as shown in figure 4.

The stationary flow-surveying instruments used were of the type shown in figure 5. One instrument was placed $1\frac{1}{2}$ inches upstream of the rotor for all runs and the other, $1\frac{1}{2}$ inches downstream for all runs except those using rotor-mounted instruments. For these tests, the downstream instrument was placed $4\frac{1}{2}$ inches downstream to prevent interference with the rotor-mounted rake and probe, figures 6 and 7, which were mounted 3 inches downstream of the blades on opposite sides of the rotor spindle. The design details and calibrations of the rotor-mounted probe are presented on figures 32 and 33 of reference 4. The rotor-mounted instruments were designed to deflect less than 0.005 inch due to centrifugal forces. The threaded sleeves, soldered to the streamline shafts, were used for mounting, angular setting, and radial adjustment of the probes at the three positions used.

A sealed-ball-bearing type pressure-transfer device, reference 5, was mounted within the test blower to transfer readings from the rotor-mounted instruments to stationary leads that were passed through the side of the annular diffuser and connected to the manometer board. For most tests, a vertical multitube alcohol manometer was used to indicate the pressure readings. However, at the low speeds used to obtain the performance at low Reynolds numbers, a calibrated manometer set at an angle of 84.25° from vertical (giving a magnification factor of ten) was used to read the very low pressure differences.

Testing methods.- When the test compressor was assembled for each condition, care was taken to keep internal surfaces evenly faired, clean, and free of surface roughness. The rotor was run up to the test speed, usually 2400 rpm, and held within ± 5 rpm during the test. Surveys upstream and downstream of the rotor were made simultaneously. The instruments were located at different circumferential positions to prevent interference. Sixteen survey positions spaced to indicate the complete

flow pattern from inner to outer casing were normally used. Static-pressure, total-pressure, and yaw readings were taken at each survey position.

The rotor-mounted instruments were set at the design outlet angle for each radial position at which they were placed and tests over a range of flow rates were run without further adjustment. Although the outlet angle varied only $\pm 3^\circ$, no significant errors were introduced. The indicated outlet flow angle from these tests was determined by using a yaw-calibration curve. Inasmuch as yaw-calibration tests indicated less than 1/4-percent variation as the probe was yawed 3°, the total-pressure and static-pressure readings were only corrected for inherent probe errors at 0° yaw (fig. 33 of ref. 4).

Test program.- Six configurations were tested with constant annulus area: for the design setting (see table I), for $7\frac{1}{2}^\circ$ above the design setting, and for $7\frac{1}{2}^\circ$ below the design setting at pitch-section solidities of 1.00 and 0.50. The quantity-flow coefficients, at design angles of attack, for the design setting, $7\frac{1}{2}^\circ$ above design, and $7\frac{1}{2}^\circ$ below design are 0.640, 0.476, and 0.830, respectively. The configuration with a blade-angle setting $7\frac{1}{2}^\circ$ above design at a pitch solidity of 1.00 was tested with ratios of rotor-exit annulus area to rotor-entrance annulus area of 1.15, 0.85, and 0.70. All tests for these conditions were made at rotor rotational speed of 2,400 rpm. The Reynolds number effect tests were made with the configuration having a constant annulus area, a blade angle at $7\frac{1}{2}^\circ$ above the design setting, and a solidity of 1.00 at various rotor speeds from 400 to 2,400 rpm. The rotor-mounted-instrument tests were also made with this latter configuration, the rotor-mounted probe and rake being located alternately at the inboard, pitch, and outboard sections corresponding to the 30-, 50-, and 70-percent-annulus-height positions, respectively. These tests were made at a rotor speed of 2,000 rpm to reduce the stresses on the rotor-mounted instruments without significantly reducing the Reynolds number. Tests were made at numerous flow rates from the maximum value obtainable to a condition near stall except for the Reynolds number effect tests, when only values near design were used.

Precision of results.- Flow instruments were calibrated in an 8-inch calibration tunnel. The static-pressure-calibration factors used gave results correct to within 1/4 percent of the dynamic pressure. The yaw null points were determined; the instruments and holders were mounted; and readings were taken with a precision believed to provide measured flow angles within $1/4^\circ$ of the actual values. The tachometer was checked with a stroboscope at line frequency and found to be accurate within 5 rpm or 1/5 percent for normal testing speeds.

The manometer was read to the nearest 0.01 inch of alcohol, which corresponds to approximately 0.1 percent of the dynamic pressure at average test conditions. For the low Reynolds number tests, the inclined manometer board permitted readings to the nearest 0.001 inch of alcohol, or about 1 percent of the dynamic pressure at the lowest speed and flow rate used.

The data were processed by an automatic computing machine. The various integrations required were also performed by the machine using arithmetic averaging. Computing-machine integrations checked continuous integrations within 1 percent.

Estimates of rotor performance were based on porous-wall cascade data. Cascade test results were corrected by interpolation and extrapolation of the available data to the conditions for which they were compared.

The measured mass-flow errors for the constant-area condition, figure 8, show that the maximum error is less than 3 percent and the average error is approximately 1 percent. For the varying-area conditions, figure 9, the maximum error is less than 5 percent and the average error is less than 3 percent. On the basis of this check and the other testing accuracies noted, it is believed that the faired curves indicate true values within 2 percent for the efficiency and pressure-rise coefficients, and within $1/4^\circ$ for the deflection angles at all conditions except near stall. This accuracy is further verified by the close checks obtained when reruns were made during the rotor-mounted instrument tests.

RESULTS AND DISCUSSION

Tests With Varying Solidity and Blade Angle

Efficiency and pressure-rise coefficients.- The performance results of the rotor at the pitch solidities of 1.00 and 0.50 for blade angles at the design, $7\frac{1}{2}^\circ$ above design, and $7\frac{1}{2}^\circ$ below design are presented jointly to simplify comparisons. The adiabatic efficiencies measured at these six configurations are shown in figure 10. The faired curves indicate relatively high values at all but extreme flow rates. A peak value of 98 percent is indicated at the design configuration. When the solidity was reduced to 0.5, the peak efficiency at design was 95 percent. The efficiency is highest at the low blade angles. The total- and static-pressure-rise coefficients along with those estimated from cascade turning-angle data for the two solidities at the design blade angle are shown in figure 11. These estimated curves assume no losses, so measured values would normally be lower. However, later figures show that the turning angles produced by the rotor were a little higher than the estimated values, so the pressure-rise coefficients should be slightly higher than estimated. Very close agreement is observed.

An attempt was made to estimate the efficiency by using cascade L/D values and a procedure suggested in reference 6. Reference 3 presents the method of calculating the cascade c_l and c_d values used for these efficiency estimations. The efficiency calculation, briefly described in the appendix, includes only blade profile losses and neglects casing boundary-layer effects. The estimated efficiency curve for the configuration with solidity of 1.00 and a blade angle $7\frac{1}{2}^\circ$ above design is compared with the measured values in figure 12 and is shown to be lower. Efficiencies were estimated by this same method using the L/D values calculated from the data measured with the rotor-mounted instruments and are seen to be higher. It is evident that the cascade L/D values are conservative. They are considerably lower than rotor measured values and more than offset the casing losses neglected. This condition may occur because the cascade values were obtained at a Reynolds number of about 250,000, whereas the Reynolds number of the rotor tests was about 500,000. At these lower Reynolds numbers laminar separation increases the drag values, and, hence, decreases the L/D ratios. In figure 13 is a comparison of blade wake profiles which indicates that cascade drag values would be more like those of the rotor if cascade data taken at a Reynolds number near 500,000 were used. A lack of systematic cascade data prevented efficiency estimations based on L/D ratios at a Reynolds number of 500,000. It is believed that the estimated curve using rotor measured profile losses would closely agree with the overall measured efficiencies if the casing losses were included. The presence of these casing losses is shown by the curve in figure 14, in which blade-element efficiencies calculated for each survey point are plotted for a typical test near design quantity flow.

Turning angle.- Figure 15 presents the measured flow turning angles at the inboard, pitch, and outboard sections for two solidities as compared with values estimated from cascade tests for these six configurations. In all instances, the rotor results are higher by 1° to $1\frac{1}{2}^\circ$. Since this indicated difference was so consistent, the possibility of measuring errors due to the effect of the wakes upon the stationary instrument was investigated. The flow downstream of a rotating blade row is discussed in reference 1. However, no method of calculating this effect resulted in corrections larger than 0.2° or 0.3° assuming normal wake profiles, so it was decided to measure the outlet angles directly for a given configuration with rotor-mounted instruments. Figure 16 shows the results of this investigation. The directly measured turning angles compare very closely with the values computed from data obtained by the stationary instruments at the outboard station and vary less than a degree at the pitch and inboard stations up to an angle of attack of 16°. Thus, the actual deflections are 1° to $1\frac{1}{2}^\circ$ higher than estimated values and reasonably true readings were obtained with the stationary instrument. An explanation of the differences is suggested by the fact that the rotor

drag coefficients are lower than the cascade drag coefficients as shown in figure 16. Since the rotor wakes were smaller, the main flow more closely follows the trailing-edge blade contour and consequently experiences a higher turning angle. The wakes in the central portion of the blades can easily be smaller, for unlike the cascade, the rotor-blade boundary layers can flow toward the inner or outer casing along the blade surfaces propelled by either centrifugal force on the boundary-layer particles or the static-pressure gradient in the main field, whichever predominates. Reference 1 discusses this action in greater detail. In addition, figure 13 indicates that if the cascade data had been at the Reynolds number of the rotor tests, 500,000, instead of 250,000, the drag values and, hence, turning-angle values would have agreed more closely with the rotor results.

In figure 17, the variation of turning angle with air inlet angle at constant angle of attack is presented to supplement cascade data where interpolation between inlet angles is required. Estimated curves are again included for comparison and it can be seen that they follow the same trends as in the rotor but at 1° to $1\frac{1}{2}^\circ$ lower turning angles as before.

In order to illustrate typical distributions of flow angles and pressure-rise coefficients across the annulus from inner to outer casing, figures 18 and 19 were prepared. Both measured and estimated values at flow rates near design for the design-blade-angle condition operating at solidities of 1.0 and 0.5 are presented. Measured turning angles that are larger than the estimated values and the resulting effects on the outlet angle and pressure-rise coefficients are again evident at all points free of the casing boundary layers.

Exit axial velocities.- The operation of this free-vortex rotor at off-design conditions resulted in a radial variation of exit axial velocities, exclusive of the boundary layers, at the various sections. In reference 7, a method of estimating the axial velocities is presented. In the use of the method, it is necessary to estimate the outlet flow angle expected so that a final result can be obtained. Two systems of estimating these angles were used and the calculations made for five of the tests at a solidity of 1.0 at each of the three different blade-angle settings. The first method makes use of the turning angles estimated from cascade tests in determining outlet angles and the second, Constant's rule, reference 8, which for the present investigation was interpreted to mean that the outlet angles are constant at the design values regardless of inlet conditions ($d\theta/d\alpha = 1$). Figure 20 indicates the difference in $d\theta/d\alpha$ values obtained from test compressor results (average of the values at the inboard, pitch, and outboard sections), cascade results (for medium-camber 65-series airfoils at conditions similar to those in the test compressor), and the interpretation of Constant's rule. Although some point checks are not exact, the trends of the test-compressor

and cascade results are similar and the agreement between the two is considered good. Figure 21 presents comparisons of measured and estimated outlet axial velocities. The operating conditions evidently are near enough to design so that the axial velocities do not depart far from constant values. However, the trends observed are in good agreement with the calculations when either outlet-angle-estimation system is used in the calculations.

Tests With Varying Annulus Area

In order to determine the effects of varying the axial velocity through compressor blade rows, one blade-setting condition was tested with fairings attached to the rotor hub to increase or decrease the axial velocity through the blades. The condition of a solidity of 1.0 and a blade angle $7\frac{1}{2}^\circ$ above design was selected for study. Some of the results previously discussed for this condition with constant annulus area are included in several of the following figures which show the rotor performance with nonconstant annulus area for convenience in making comparisons. Figures 22 and 23 present the efficiencies and pressure-rise coefficients measured at ratios of rotor-exit annulus area to rotor-entrance annulus area of 1.15, 0.85, and 0.70 as compared with the constant-area results. For $A_2/A_1 = 1.0$, the peak efficiency is about 97.5 percent as compared with 93, 96.5, and 97.5 percent for $A_2/A_1 = 1.15$, 0.85, and 0.70, respectively. Within the limits of measuring accuracy, the efficiencies increase as the static-pressure-rise decreases. The total-pressure-rise coefficients for the several area ratios, when plotted against flow coefficient, figure 23, are seen to differ considerably, particularly for $A_2/A_1 = 0.70$. At a quantity coefficient of 0.52, the total-pressure-rise coefficients at $A_2/A_1 = 1.15$, 1.00, 0.85, and 0.70 are 0.60, 0.665, 0.575, and 0.355, respectively. Because of the large difference in mean velocity for the different area ratios, the quantity coefficient is probably not the best basis on which to compare total-pressure rise. A better basis might be the effective angle of attack α_e which is based on the mean axial velocity. In figure 24, the total-pressure-rise coefficients ψ_T are plotted against the effective angle of attack. Near the design angle of attack the difference between the ψ_T values for $A_2/A_1 = 0.85$ and 1.0 is very small (approximately 2 percent of ψ_T at $A_2/A_1 = 1.0$); whereas, the difference between the ψ_T values for $A_2/A_1 = 1.15$ and 1.00 is not as small (approximately 7 percent of ψ_T at $A_2/A_1 = 1.0$). The increased diffusion with $A_2/A_1 = 1.15$ decreases the efficiency and, hence, decreases ψ_T. The change in tangential velocity ΔV_{tan}, which is proportional to ψ_T for constant efficiency, is about the same near the design angle of attack for a

15-percent decrease in annulus area as for constant annulus area through the rotor. Evidently the effective turning angles near design are nearly the same for the same effective angle of attack even though the area change considerably alters the inlet and outlet air angles. The static-pressure-rise coefficient is greatly affected, however, and is largely dependent on the area ratio as should be expected.

The curves of α against θ at these four annulus-area ratios for the inboard, pitch, and outboard sections are given in figure 25. The measured turning angles vary greatly from the values estimated from cascade tests for $A_2/A_1 = 1.00$. The variation is systematic, but differences in turning as much as 4°, around design angle of attack, exist when the annulus-area ratio is 15 percent above or below 1.00. The difficulty of estimating directly the turning angles of blade rows having annulus-area ratios other than 1.0 from constant-area cascade results has been known for some time. However, methods have been suggested to combat this difficulty.

One method of converting the data to two-dimensional-flow conditions is to assume that the effective outlet angle is found if the outlet axial velocity is taken to be the same as the inlet value, the outlet tangential velocity not being changed, see vector diagram in figure 26(a). This assumes a constant circulation. This correction system was applied to these tests and the resultant curves of α against θ are shown in figure 27. Cascade curves also corrected in this same manner are included for comparison. The system is seen to result in a large over-correction in every instance with the discrepancies nearly as large as those of the initial uncorrected values. Consequently this system does not appear to be valid.

A second method of correction is to retain constant circulation but to correct both inlet and outlet angles to the mean axial velocity. This of course introduces a different value for both α and θ, as indicated in the diagram of figure 26(b). The results using this system are shown in figure 28 with estimated curves corrected in the same manner. The agreement is much better but careful observation reveals that this is also an over-correction system.

In an ideal system, all the curves, regardless of axial-velocity change, would fall upon the constant-annulus-area line. Although correction to an axial velocity of magnitude between the mean and outlet value would nearly produce this ideal result for these tests, it is not believed that this same correction would be optimum at other ranges of inlet air angle or for other methods of producing a change in axial velocity through blade sections. Therefore, a more fundamental system must yet be devised if high accuracy at all conditions is desired. At present, the mean-axial-velocity system appears to yield results of

sufficient accuracy for most applications in which axial-velocity changes up to about 15 percent occur.

The mean-axial-velocity correction system was used to estimate from cascade tests the pressure-rise coefficients and flow angles across the annulus for a test near design inlet air angle at each of the four area ratios. These estimations are compared with measured values in figures 29 and 30. For the area ratios of 1.00 and 0.85, the comparisons are nearly exact. The differences in flow angles and pressure-rise coefficients evident for $A_2/A_1 = 1.15$ probably result from the local effects of fairings and increased boundary-layer thickness due to the severe static-pressure rise across the rotor. The configuration with $A_2/A_1 = 0.70$ has a very low estimated static-pressure-rise coefficient, 0.21 compared to 0.56 for the configuration for which $A_2/A_1 = 1.0$, so the low values of total-pressure-rise coefficient cannot logically be attributed to thick boundary layers. More likely, the assumption of constant circulation for this case of increasing axial velocity through the rotor is unsound.

Since the outlet axial velocities for these area-change tests were quite different from the previous tests, a comparison was made between measured values and those estimated using the system of reference 7. This comparison was made for one test near the design inlet air angle for each area change condition, see figure 31. The measured trend is again estimated quite well by the system using either cascade data or the interpretation of Constant's rule for estimating outlet air angles.

Tests of Varying Reynolds Number

The rotor speed, quantity-flow coefficient, and resultant mean section Reynolds number of the tests made to investigate the effects of Reynolds number are shown in figure 32. The design flow coefficient, 0.476, is also indicated in the figure. The Reynolds number at design flow for given speeds was used in the preparation of the other graphs. The adiabatic efficiency is shown in figure 33. The scatter in results is believed due to testing inaccuracies illustrated by the errors in measured mass flows as also shown in this figure. The trend is quite definite, however, indicating an appreciable decrease in efficiency below R = 250,000. A comparison curve, estimated using cascade results and the equation of reference 6, shows close agreement in trend and absolute values. Because it is computed using only data for an NACA 65-(12)10 section and it does not include casing losses, the estimated curve is expected to be higher and at best an approximation. The total- and static-pressure-rise coefficients, figure 34, also show a decrease with reduced Reynolds number. The reduction is 10 to 15 percent for both curves, but no definite Reynolds number below 400,000 can be described

as the "drop-off point." The curves of turning angle against Reynolds number, faired at a design quantity-flow coefficient of 0.476 for the inboard, pitch, and outboard sections, figure 35, show unexplained trends. A gradual reduction is observed as the Reynolds number is decreased from 400,000 to 150,000. At R = 150,000, the trend reverses and at R = 80,000, a return to values measured at higher Reynolds numbers occurs. The estimated curve for the inboard section follows this trend to the point of reversal. Cascade data for lower Reynolds numbers are not available. The displacement of the estimated curve from the measured curve by 1° to $1\frac{1}{2}^\circ$ is in agreement with the comparisons made in figure 15. Similar turning-angle results at these lowest Reynolds numbers have been observed in other unpublished investigations.

CONCLUSIONS

An investigation of a typical axial-flow compressor rotor over a range of quantity flow rates, blade angles, annulus-area ratios, solidities, and Reynolds numbers was made and the performance compared to values estimated using porous-wall-cascade data. As a result of this study, it is concluded that:

1. Low-speed cascade results can be used to estimate rotor turning angles, static- and total-pressure-rise coefficients and efficiencies accurately for a wide variety of conditions.

2. The mean-axial-velocity method of converting the data to two-dimensional-flow conditions can be used with good results in estimating rotor performance from cascade data for axial-velocity changes across the rotor as large as 15 percent.

3. The calculated outlet axial velocities, excluding the boundary layer, were found to be in good agreement with measured values for all comparisons made.

4. The flow turning angles produced by the test rotor were consistently higher than cascade values by 1° to $1\frac{1}{2}^\circ$ for all conditions tested.

5. The effect of decreased Reynolds number was found to be very small in the range between 250,000 and 500,000. As the Reynolds number was decreased below 250,000, decreases in rotor efficiency, pressure-rise-coefficient, and turning angle were observed. Good agreement between cascade and rotor trends was observed.

Langley Aeronautical Laboratory,
National Advisory Committee for Aeronautics,
Langley Field, Va., December 16, 1952.

APPENDIX

REDUCTION OF DATA

The relevant relationships and the methods used in calculating the performance from the test data will be presented. All performance quantities are based on entering conditions of 2,116 pounds per square foot and 519° F absolute.

The rotor inlet density for these tests was determined from the following expansion of the isentropic pressure-density relationship:

$$\rho = \rho_{ch}\left[1 - \frac{p_s - p_{s_{ch}}}{\gamma p_{s_{ch}}}\left(\frac{p_s - p_{s_{ch}}}{\frac{2\gamma p_{s_{ch}}}{\gamma - 1}} - 1\right)\right]$$

The flow was assumed to be incompressible and the power input is calculated from momentum consideration:

$$I_2 - I_1 = \rho\int_{r_h^2}^{r_t^2}\left(V_{a_2}V_{tan_2} - V_{a_1}V_{tan_1}\right)2\pi^2 nr\, d\left(r^2\right)$$

Total pressures were determined from radial survey measurements. The power output based on chamber pressure may be very closely approximated for low values of P_{T_2}/P_{T_1} by

$$E_2 = \pi\int_{r_h^2}^{r_t^2} V_{a_2}\left(P_{T_2} - P_{T_{ch}}\right)d\left(r^2\right)$$

The mass flow at each point is

$$M = \pi\int_{r_h^2}^{r_t^2} \rho V_a\, d\left(r^2\right)$$

For equal measured mass flows, rotor efficiency is

$$\eta_r = \frac{E_2 - E_1}{I_2 - I_1}$$

Since measured mass flow varied by as much as 5 percent (figs. 8 and 9) a mass-flow correction was applied to the efficiency. If the mass flow at position 2 is assumed correct and if the mass flow errors are assumed to be the result of errors in static-pressure measurement, rotor efficiency becomes

$$\eta_r = \frac{E_2 - E_1 \frac{M_2}{M_1}}{I_2 - I_1\left(\frac{M_2}{M_1}\right)^2}$$

Actually the corrections had only a minor effect because E_1 and I_1 were always close to zero.

In reference 7 theoretical equations are presented for the calculation of axial velocity distributions upstream or downstream of blade rows. If the general equation is modified for the condition of rotor tests with no guide vane and with constant inlet axial velocity (neglecting wall boundary layers), the rotor exit axial velocity distribution becomes:

$$\frac{V_{a_2}}{U_t} = \left(\cos \beta_2\right) e^{-\int_{D_h/D_t}^{D/D_t} \frac{\sin^2\beta_2}{D/D_t} d\left(D/D_t\right)} \left[\int_{D_h/D_t}^{D/D_t} 2\left(\sin \beta_2\right) e^{\int_{D_h/D_t}^{D/D_t} \frac{\sin^2\beta_2}{D/D_t} d\left(D/D_t\right)} d\left(D/D_t\right) + \left(\frac{V_{a_2}}{U_t \cos \beta_2}\right)_{D_h/D_t} \right]$$

Determination of the value of $\left(\frac{V_{a_2}}{U_t \cos \beta_2}\right)_{D_h/D_t}$ necessary to satisfy continuity requires a trial-and-error solution. As a first approximation an estimation of the pitch section axial velocity is made by using the following equation:

$$\left(\frac{V_{a_2}}{U_t}\right)_{D_p/D_t} = \left(\frac{V_{a_1}}{U_t}\right)_{D_p/D_t} \frac{A_1}{A_2}$$

The general equation can then be written for $\left(V_{a_2}/U_t\right)_{D_p/D_t}$ and solved for $\left(\frac{V_{a_2}}{U_t \cos \beta_2}\right)_{D_h/D_t}$. With this first approximation of $\left(\frac{V_{a_2}}{U_t \cos \beta_2}\right)_{D_h/D_t}$, the general equation can be used to determine the rotor exit axial velocities for several radial stations across the annulus. To satisfy continuity, the integrated area under the curves of V_{a_1}/U_t and V_{a_2}/U_t plotted against $\left(D/D_t\right)^2$ must coincide. Adjustment of the value of $\left(\frac{V_{a_2}}{U_t \cos \beta_2}\right)_{D_h/D_t}$ is made to satisfy continuity. Generally, continuity can be satisfied within 1 percent for no more than two or three adjustments of the value of $\left(\frac{V_{a_2}}{U_t \cos \beta_2}\right)_{D_h/D_t}$. In this paper the axial velocity distribution was calculated for five radial stations from root to tip.

A general method for predicting efficiencies for blade rows for which L/D values are known or may be estimated is given in reference 6. The basic equation

$$\eta = 1 - \frac{\text{Power losses}}{\text{Power input}}$$

when applied in this investigation becomes

$$\eta = 1 - \frac{1}{\left(\frac{L}{D} + \tan \beta_M\right) \tan \beta_1 \cos^2 \beta_M}$$

where

$$\beta_M = \tan^{-1} \frac{\tan \beta_1 + \tan \beta_2}{2}$$

Estimated values of L/D were obtained from the available cascade data for the values of β, α, and θ expected at various radii. In this paper this was done at the inboard, pitch, and outboard radii. The sectional efficiency at each point was calculated by using the above equation. The calculated efficiencies were plotted against radius and faired to the casings to provide an efficiency distribution across the annulus. The estimated rotor efficiencies were obtained by mechanically integrating these efficiency distributions and computing average values.

REFERENCES

1. Westphal, Willard R., and Godwin, William R.: Comparison of NACA 65-Series Compressor-Blade Pressure Distributions and Performance in a Rotor and in Cascade. NACA TN 3806, 1957. (Supersedes NACA RM L51H20.)

2. Bogdonoff, Seymour M., and Herrig, L. Joseph: Performance of Axial-Flow Fan and Compressor Blades Designed for High Loadings. NACA TN 1201, 1947.

3. Herrig, L. Joseph, Emery, James C., and Erwin, John R.: Systematic Two-Dimensional Cascade Tests of NACA 65-Series Compressor Blades at Low Speeds. NACA TN 3916, 1957. (Supersedes NACA RM L51G31.)

4. Schulze, Wallace M., Ashby, George C., Jr., and Erwin, John R.: Several Combination Probes for Surveying Static and Total Pressure and Flow Direction. NACA TN 2830, 1952.

5. Davey, Richard S.: Multiple Pressure-Transfer Device. Instruments, vol. 23, no. 4, Apr. 1950, p. 350.

6. Sinnette, John T., Jr.: Analysis of Effect of Basic Design Variables on Subsonic Axial-Flow-Compressor Performance. NACA Rep. 901, 1948.

7. Bowen, John T., Sabersky, Rolf H., and Rannie, W. Duncan: Theoretical and Experimental Investigations of Axial Flow Compressors. Summary Report, Contract N6-ORI-102 Task Order IV, Office of Naval Res., Mech. Eng. Lab., C.I.T., Jan. 1949.

8. Howell, A. R.: The Present Basis of Axial Flow Compressor Design. Part I. Cascade Theory and Performance. R. & M. No. 2095, British A.R.C., 1942.

TABLE I.- DESIGN CONDITIONS

[Description of blade sections is given in reference 3]

Section	NACA blade profile	α, deg	θ, deg	β_1, deg	β_2, deg	ξ, deg	σ	D/D_t
Original design details from reference 2								
Root	65-(13.5)10	16.7	24.1	48.8	24.7	32.1	1.135	.784
Pitch	65-(11)10	13.1	17.4	52.4	35.0	39.3	1.000	.892
Tip	65-(8.5)10	10.0	12.9	55.5	42.6	45.5	.892	1.000
Design conditions for this investigation								
Root	65-(13.5)10	15.6	24.2	48.9	24.7	33.3	1.135	.784
Inboard	65-(12)10	13.3	19.9	51.1	31.2	37.8	1.051	.849
Pitch	65-(11)10	12.0	17.5	52.5	35.0	40.5	1.000	.892
Outboard	65-(10)10	10.8	15.5	53.8	38.3	43.0	.954	.935
Tip	65-(8.5)10	8.9	13.0	55.6	42.6	46.7	.892	1.000

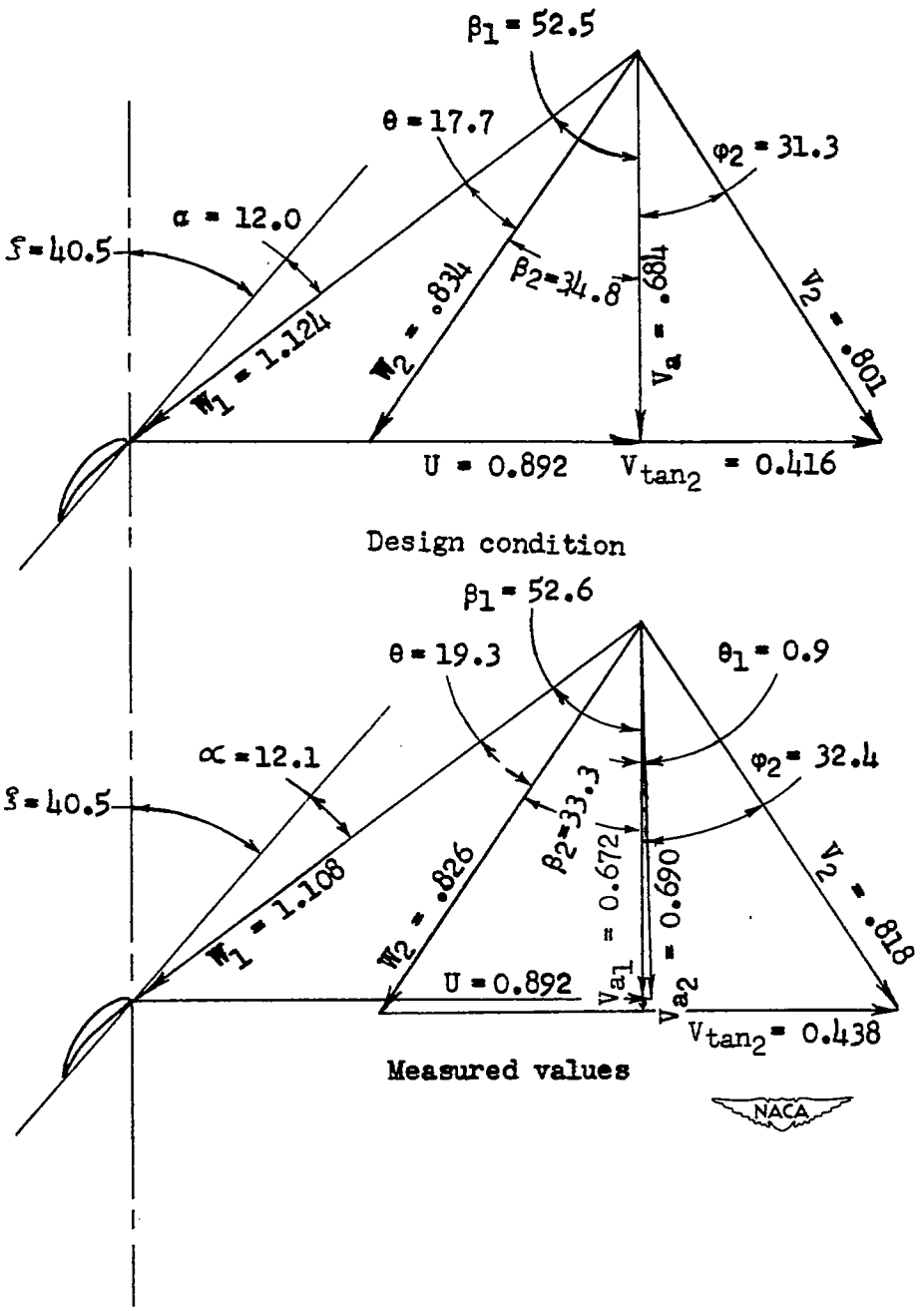

Figure 1.- Velocity diagrams at pitch section for design condition and measured values near design flow rate expressed as a fraction of U_t.

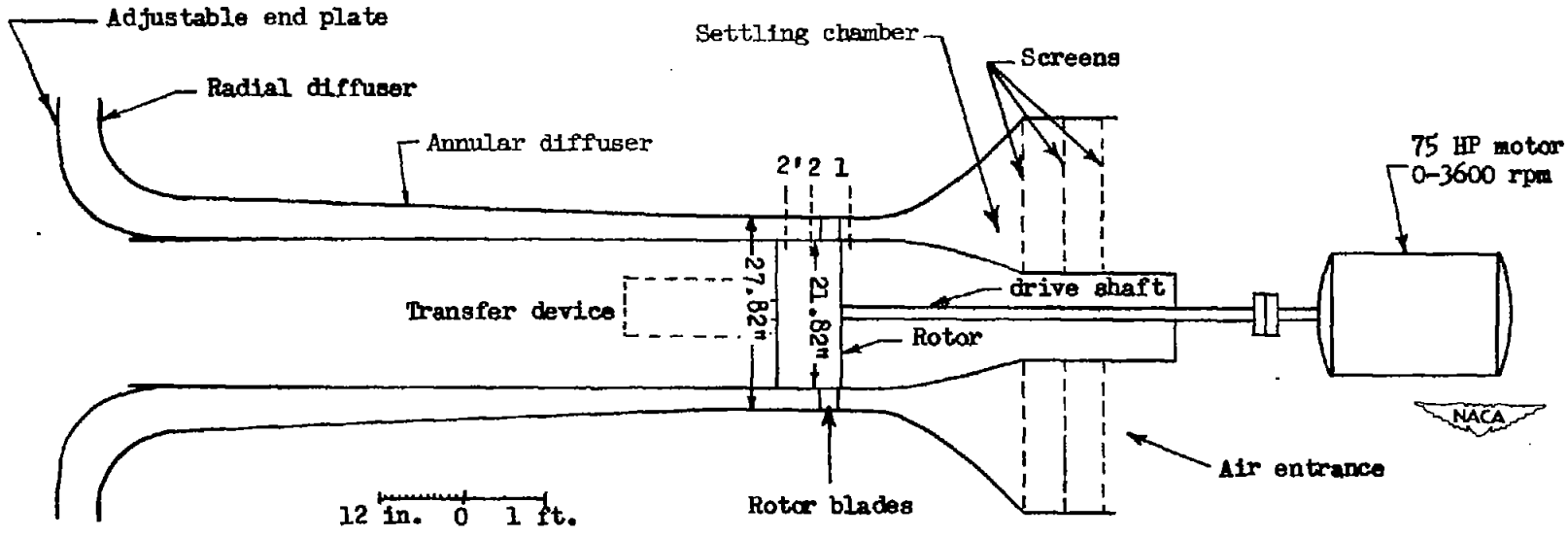

Figure 2.- Schematic diagram of test compressor showing rotor and instrumentation positions.

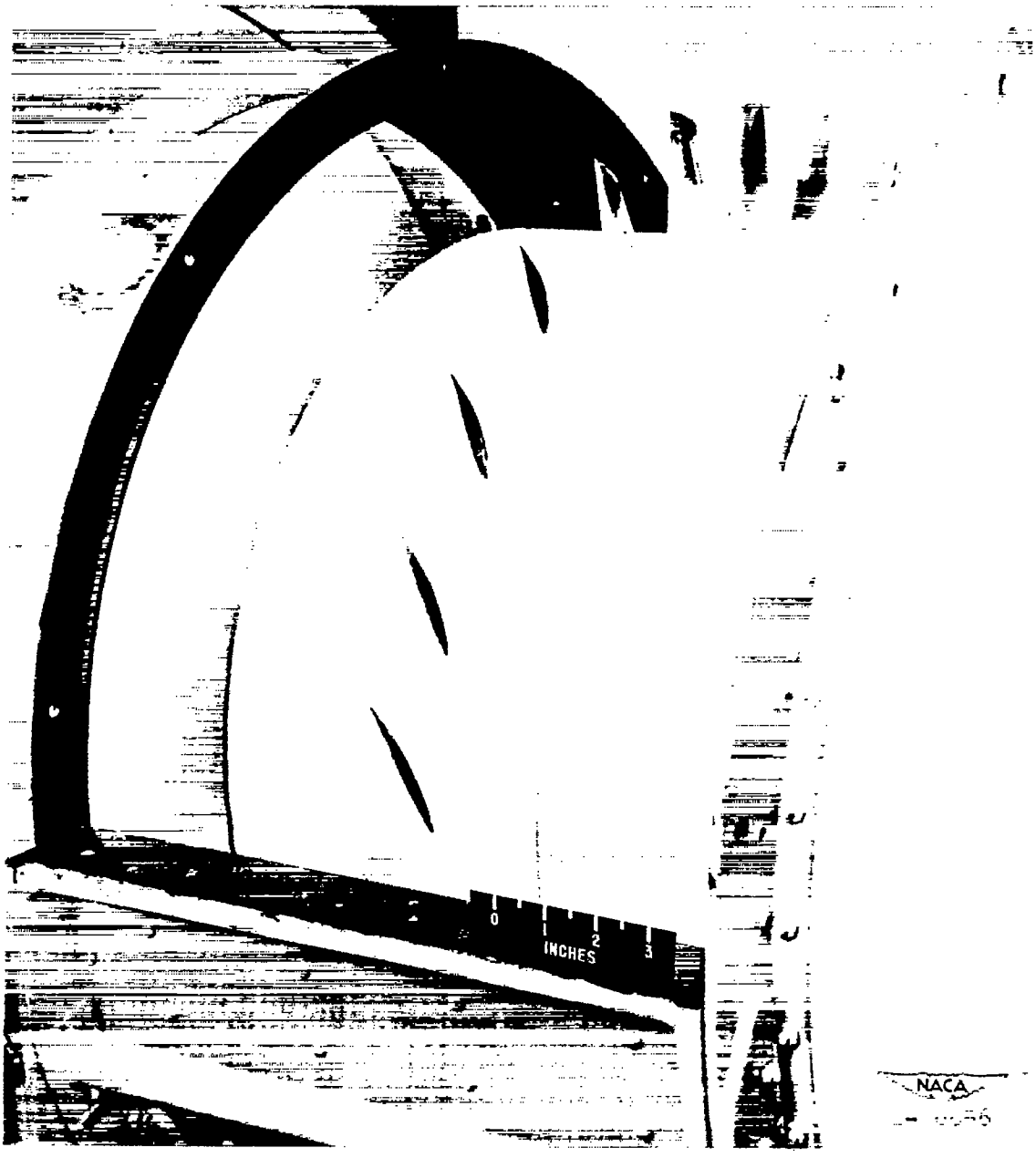

Figure 3.- Partial view of test section showing rotor configuration as altered to provide exit-to-entering annulus-area ratio of 1.15. Solidity, 1.0; $7\frac{1}{2}^{\circ}$ above design blade angle.

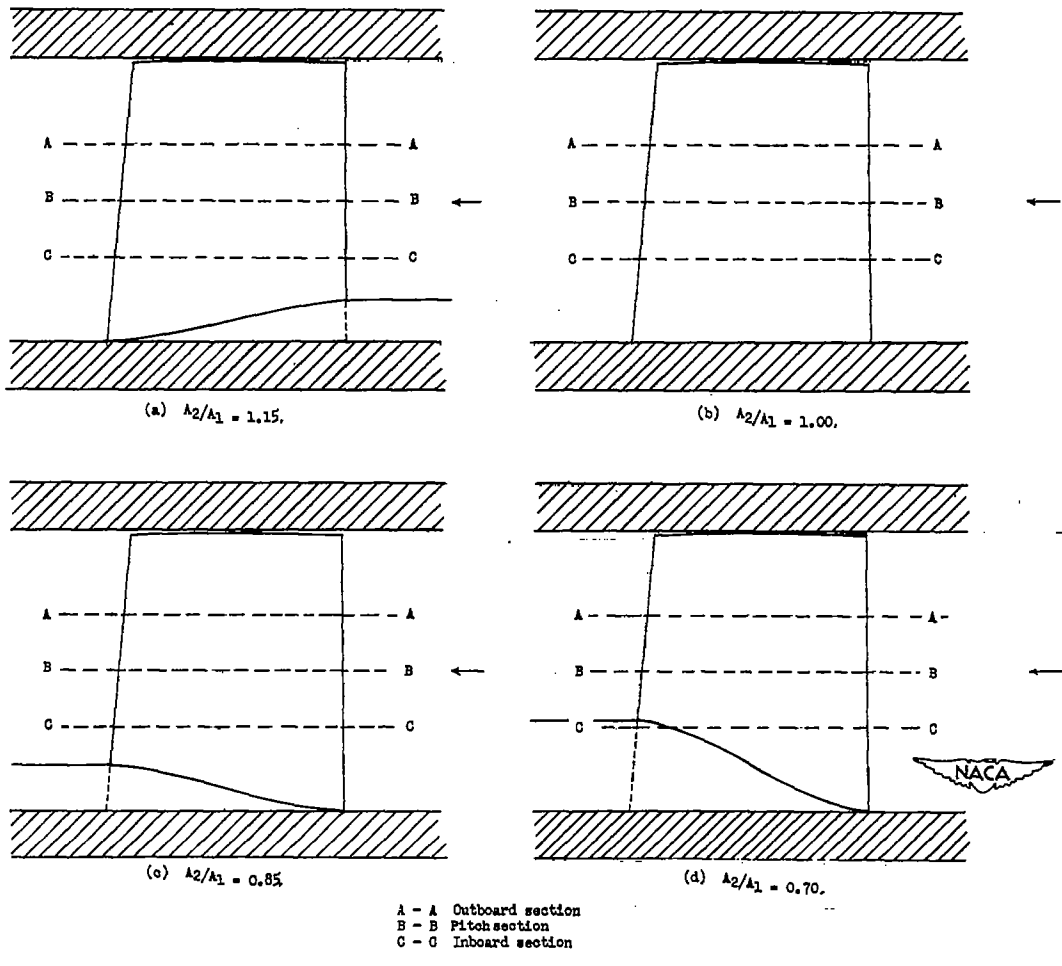

Figure 4.- Cross-sectional view through rotor illustrating the annulus-area changes tested in this investigation. The balsa fairing was made tangent to the axial direction at the leading and trailing edges of the blade and arbitrarily faired in between.

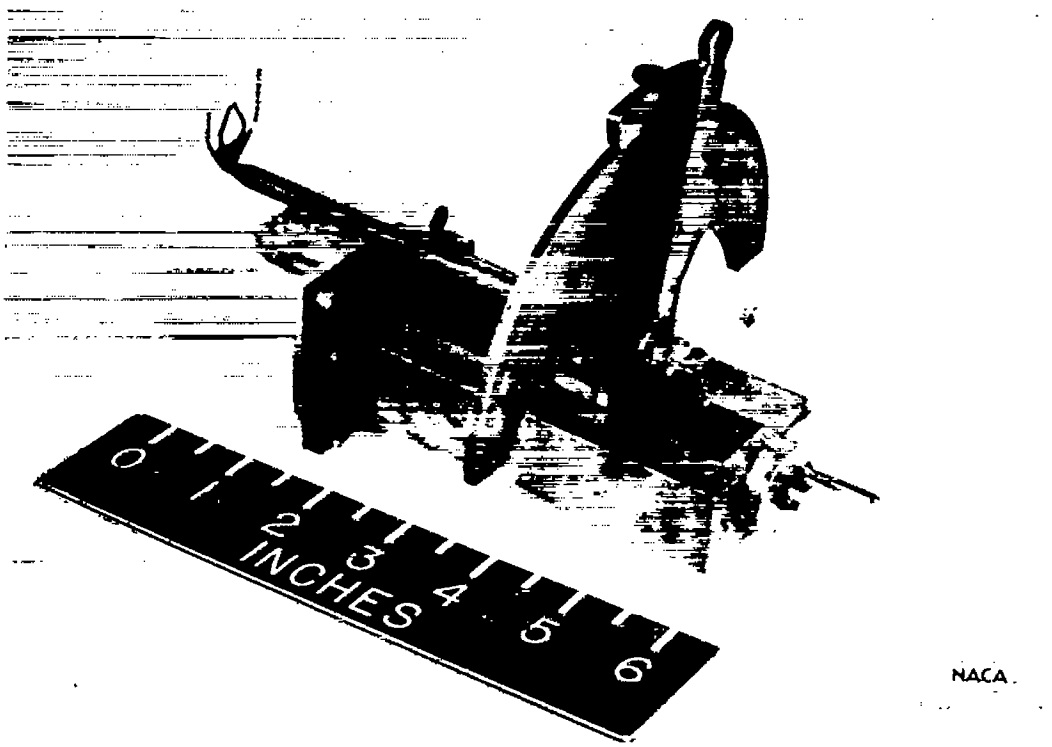

Figure 5.- Survey instrument with measuring head installed showing arrangement of yaw, total-pressure, and static-pressure tubes.

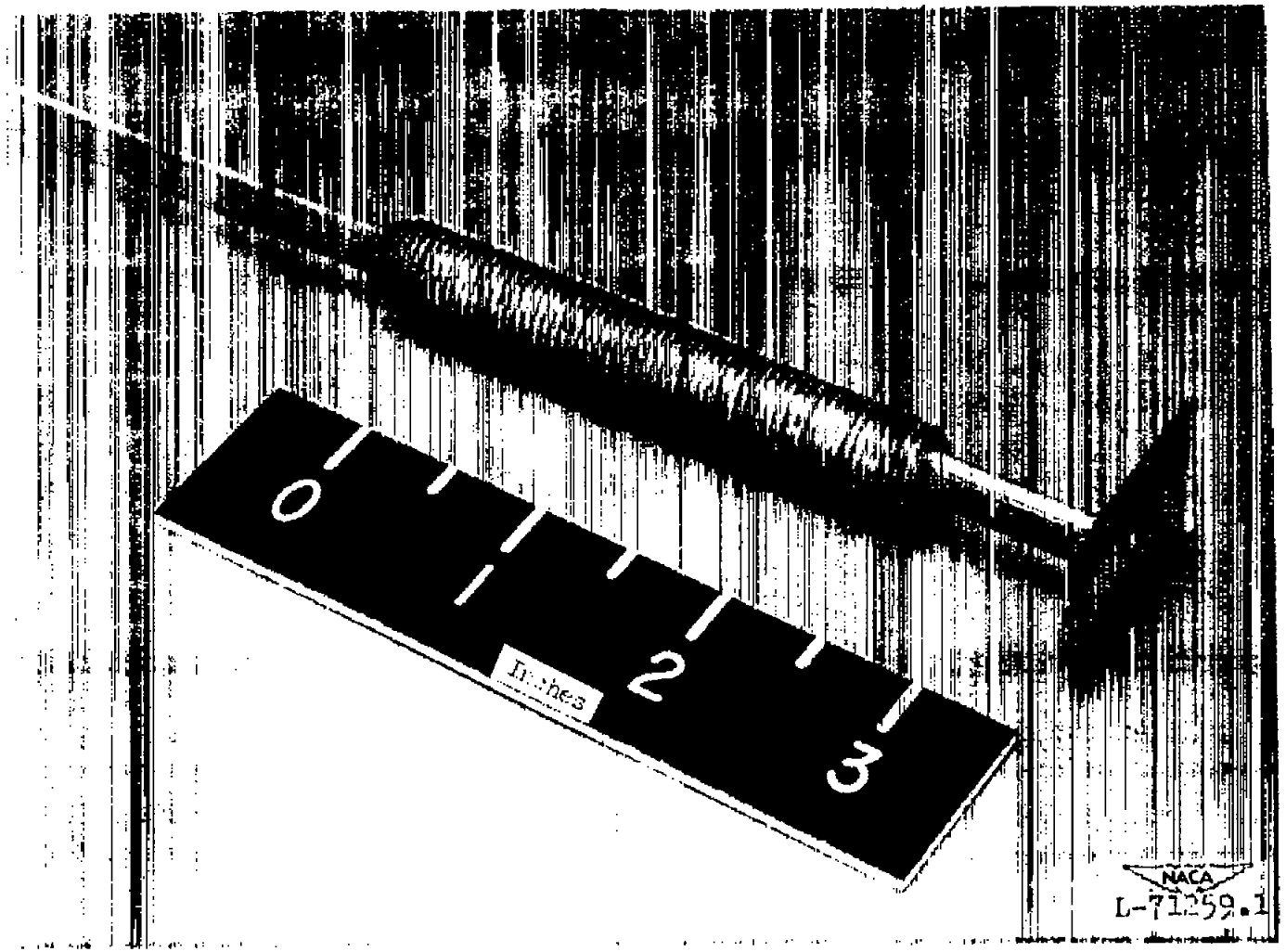

Figure 6.- Instrument used on rotor to measure blade wake profiles.

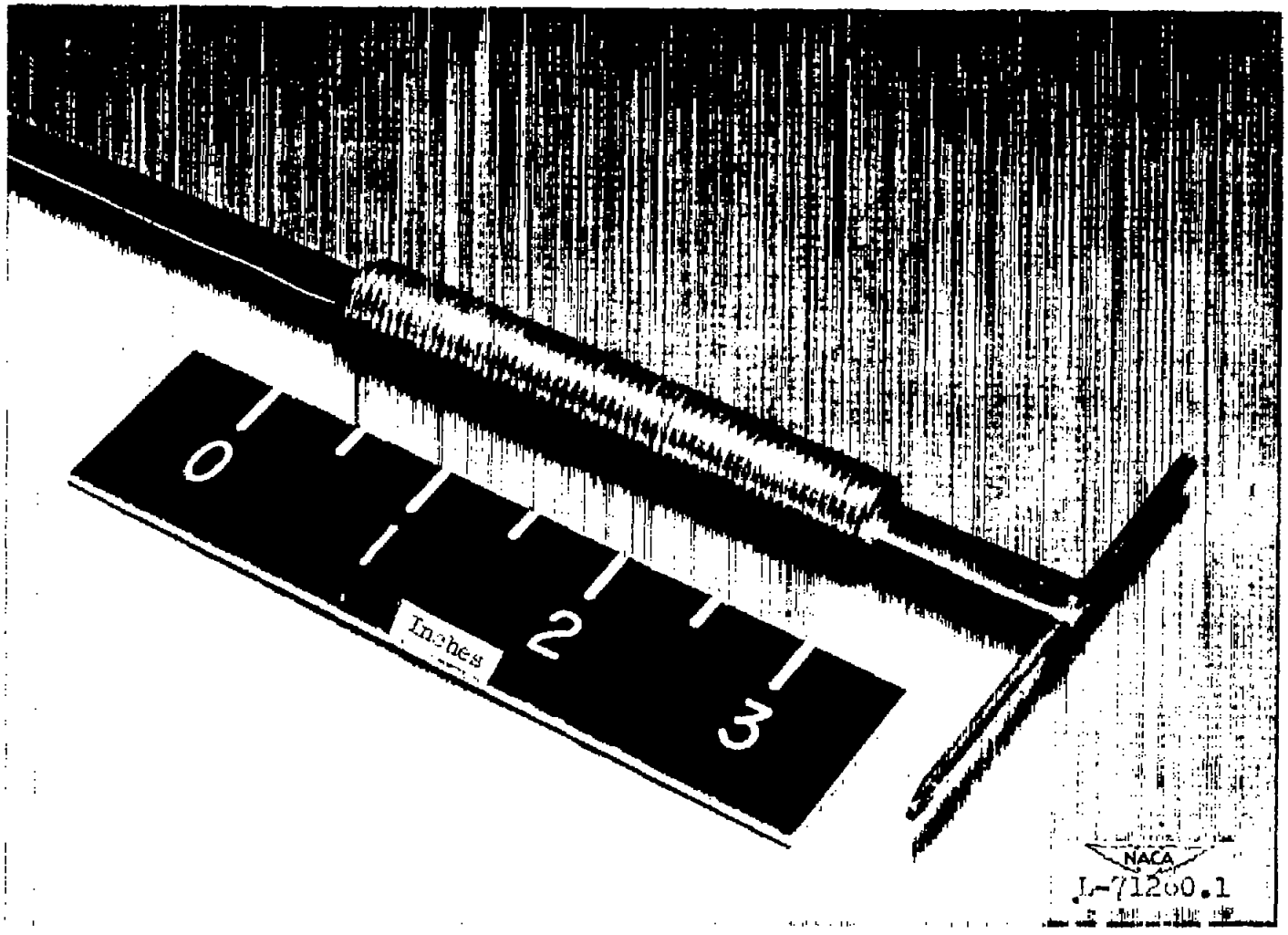

Figure 7.- Instrument used on rotor to measure static and total pressure and outlet angle.

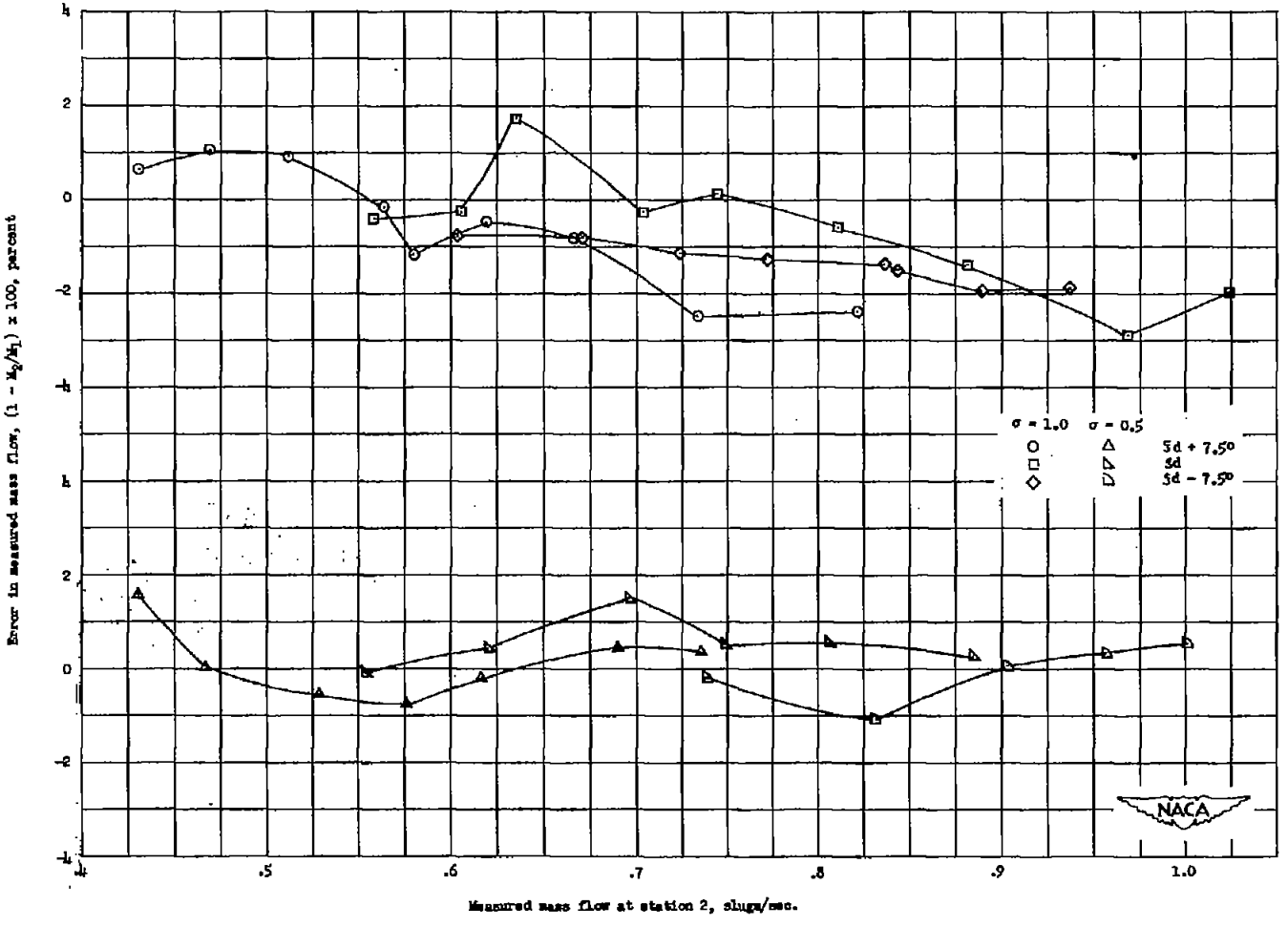

Figure 8.- Difference in measured mass flows at stations 1 and 2 for the constant-area tests with design, $7\frac{1}{2}^\circ$ above design, and $7\frac{1}{2}^\circ$ below design blade angles at solidities of 1.0 and 0.5.

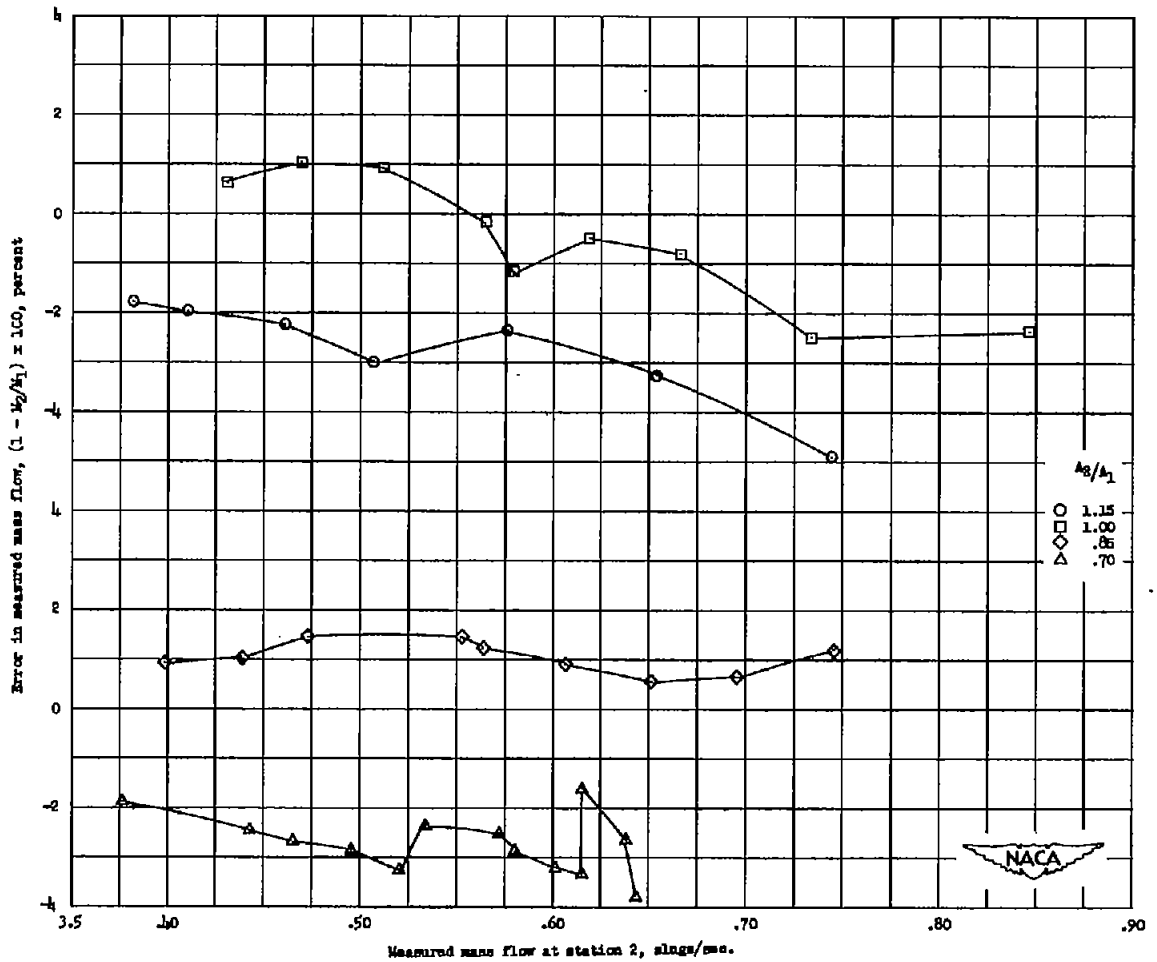

Figure 9.- Difference in measured mass flows at stations 1 and 2 for $7\frac{1}{2}^{\circ}$ above design blade angle and solidity of 1.0 with annulus-area ratios of 1.15, 1.00, 0.85, and 0.70.

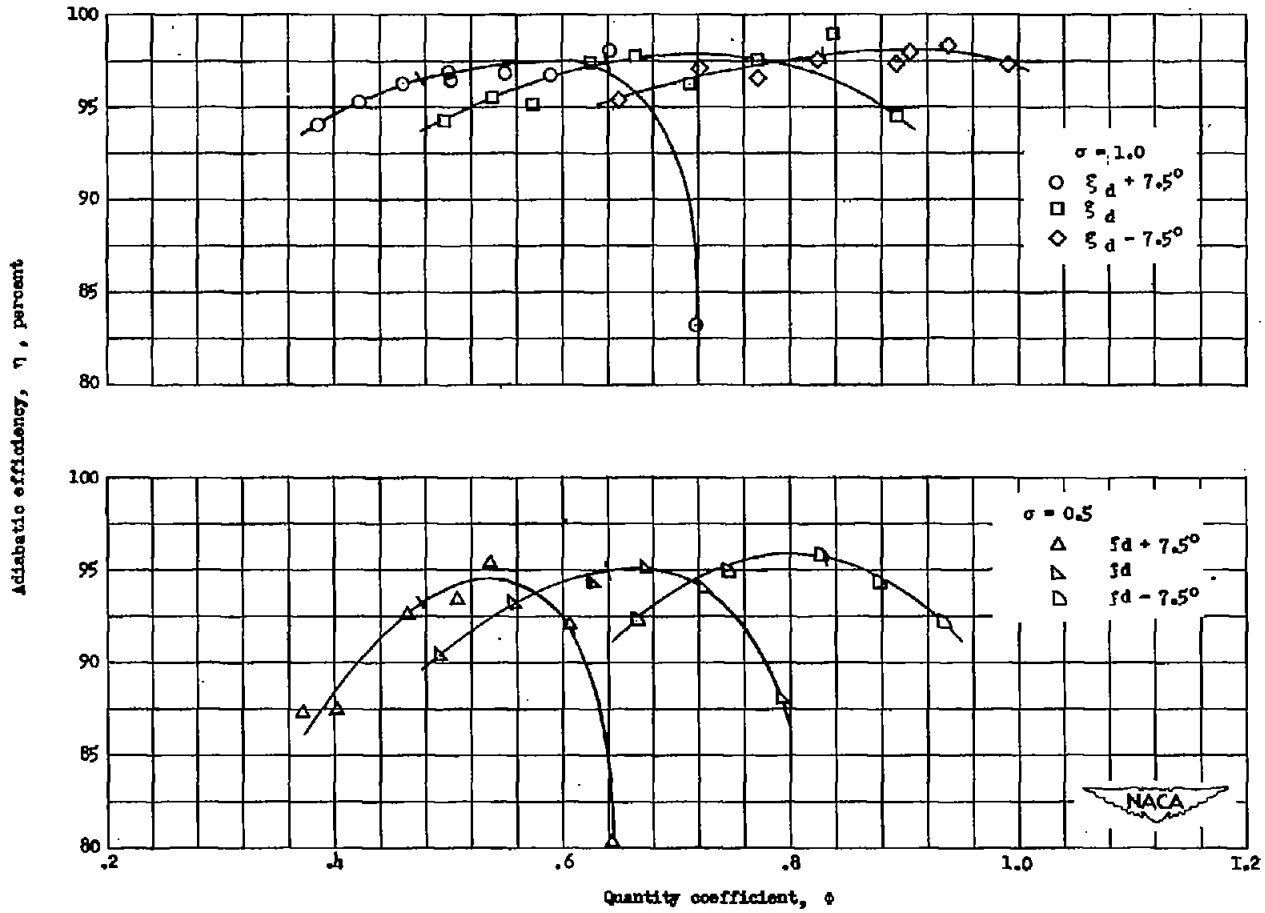

Figure 10.- Variation of adiabatic efficiency with quantity coefficient for constant-area condition with blade angles at design, $7\frac{1}{2}^{\circ}$ above design, and $7\frac{1}{2}^{\circ}$ below design settings at solidities of 1.0 and 0.5. (Lines across curves indicate design points.)

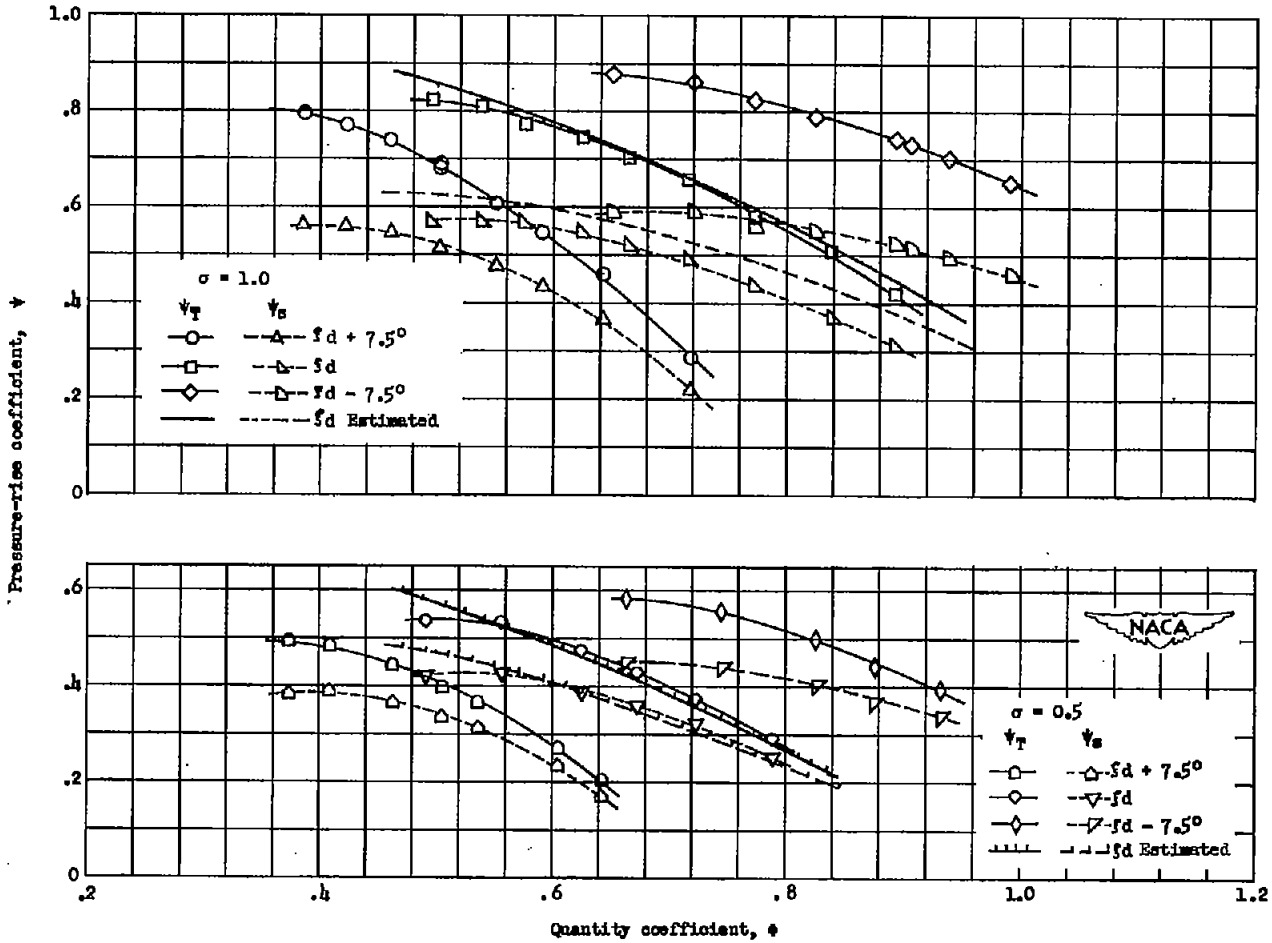

Figure 11.- Variation of total- and static-pressure-rise coefficient with quantity coefficient for the constant-annulus-area condition with design, $7\frac{1}{2}^{\circ}$ above design, and $7\frac{1}{2}^{\circ}$ below design blade angles at solidities of 1.0 and 0.5.

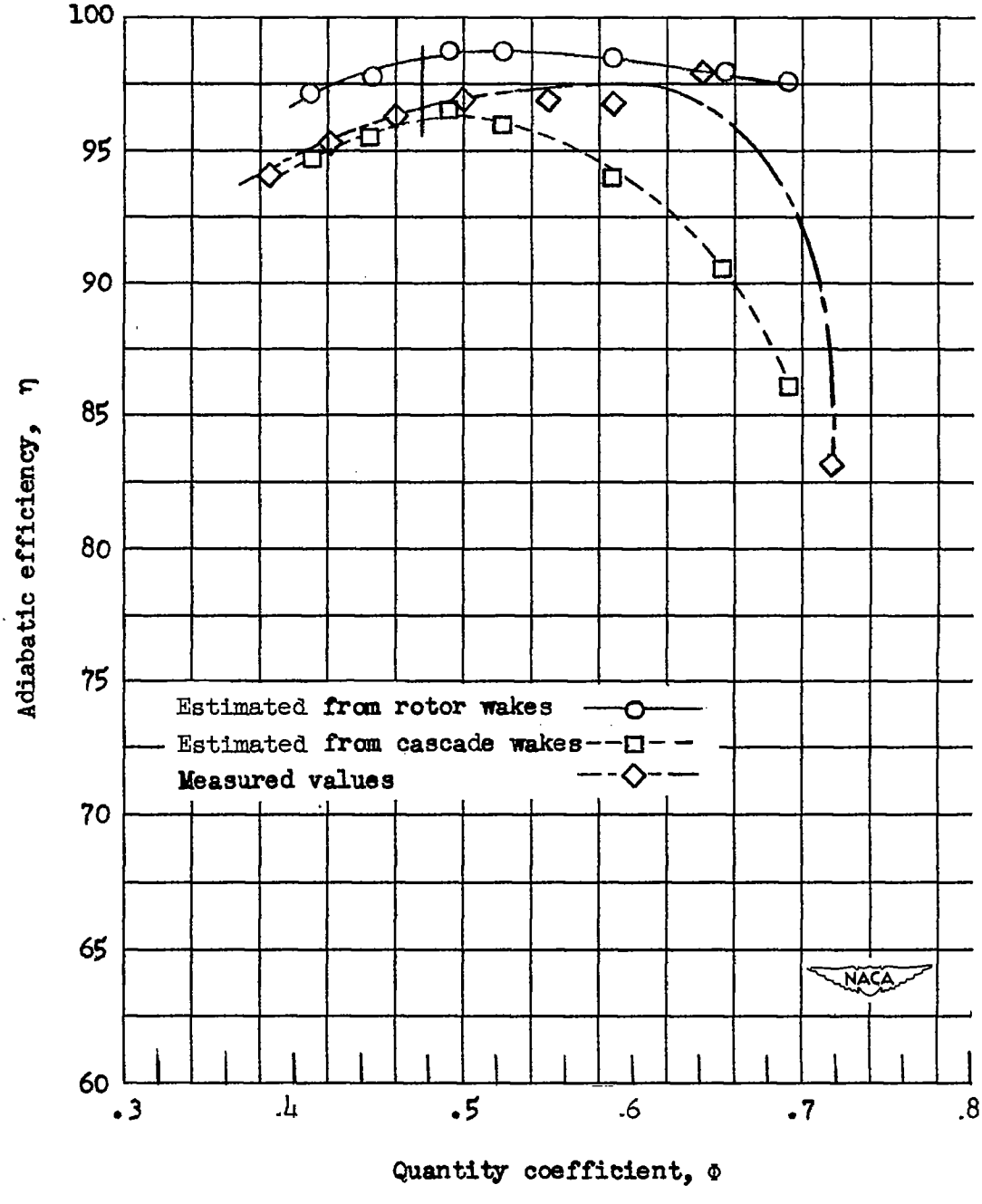

Figure 12.- Variation of measured and estimated efficiencies with quantity coefficient for constant-annulus-area condition with blade angle set $7\frac{1}{2}^{\circ}$ above design at solidity 1.0. (Vertical line across the curve indicates design point.)

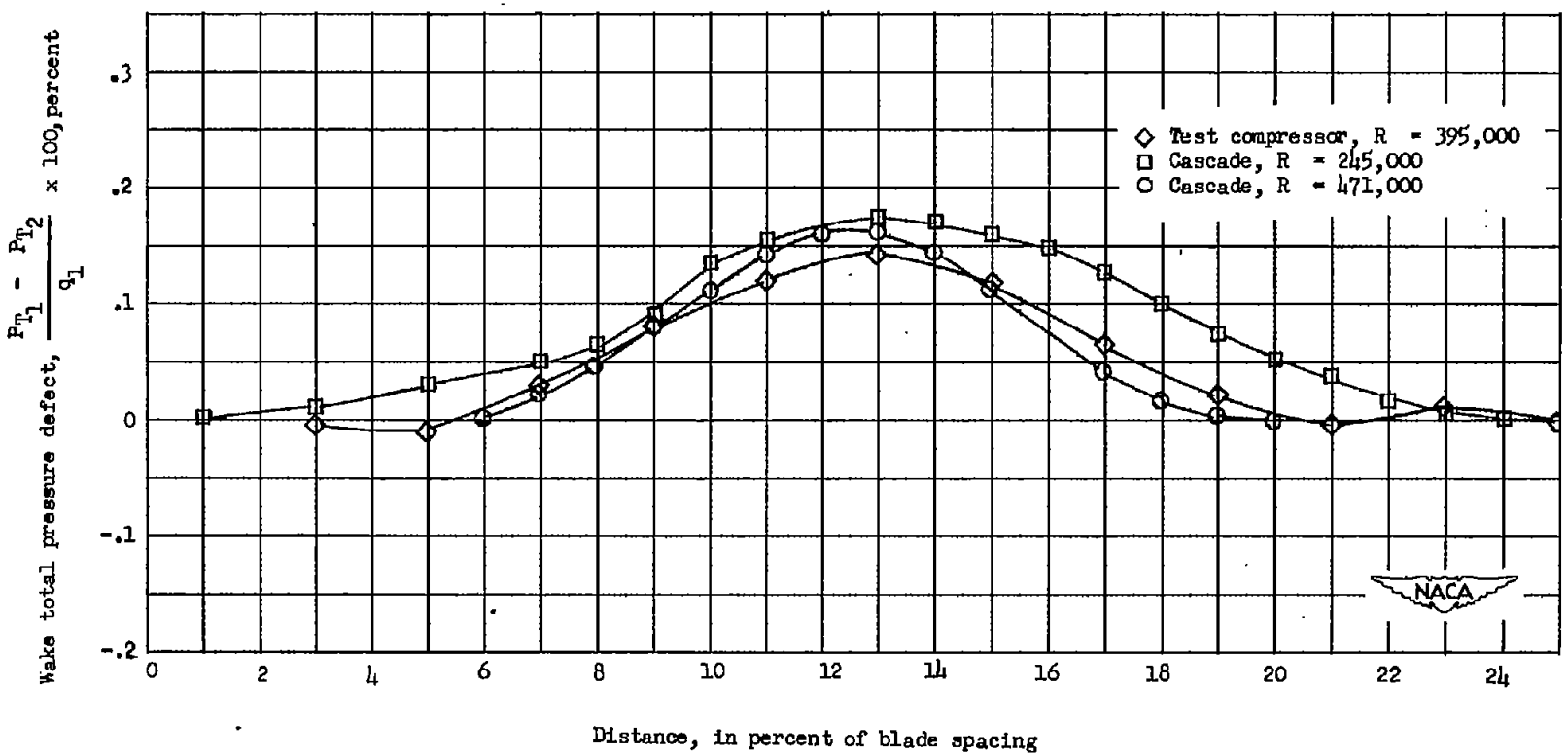

Figure 13.- Comparison of wakes measured in the test rotor at the pitch diameter and in a low-speed cascade tunnel. The rotor pitch diameter had an NACA 65-(11)10 blade section. The blades in cascade were of NACA 65-(12)10 section. $\beta_1 = 60^\circ$, $\alpha = 12^\circ$.

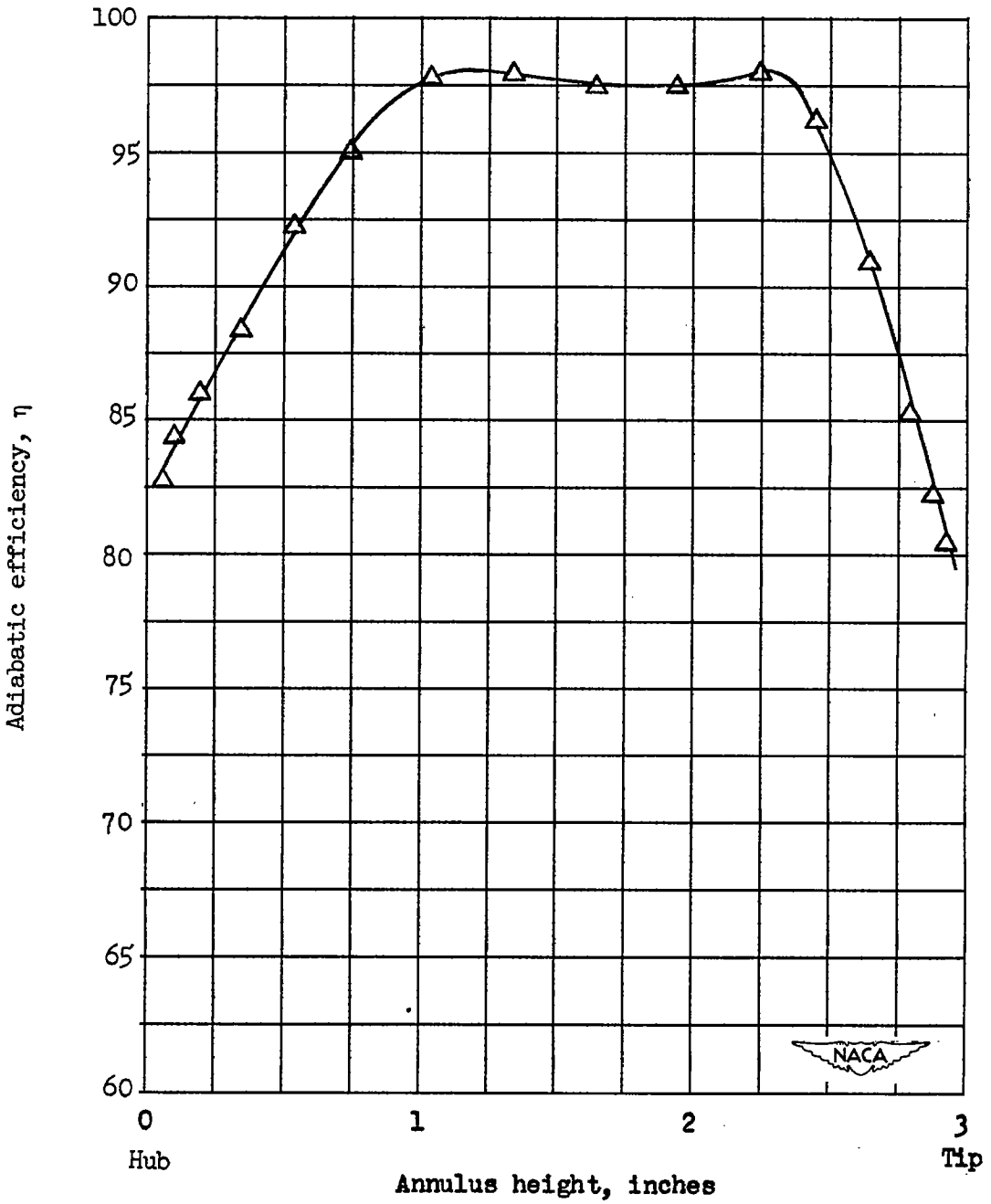

Figure 14.- Variation of efficiency across the annulus for a typical test of the constant-annulus-area condition with $7\frac{1}{2}^{\circ}$ above design blade angle at solidity 1.0. Φ approximately equal to design value.

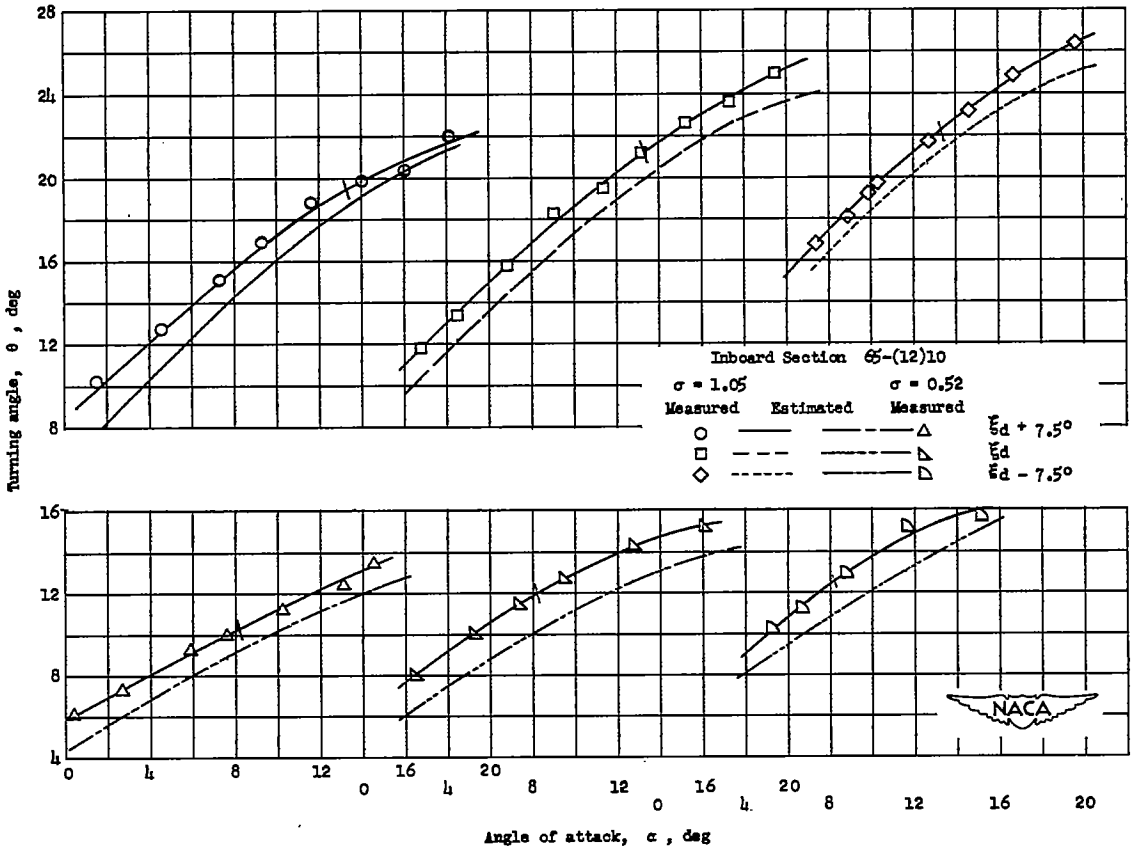

(a) Inboard section.

Figure 15.- Variation of turning angle with angle of attack as measured and estimated for the constant-annulus-area condition with design, $7\frac{1}{2}^{\circ}$ above design, and $7\frac{1}{2}^{\circ}$ below design blade angles of solidities of 1.0 and 0.5. (Bars across curves indicate design points.)

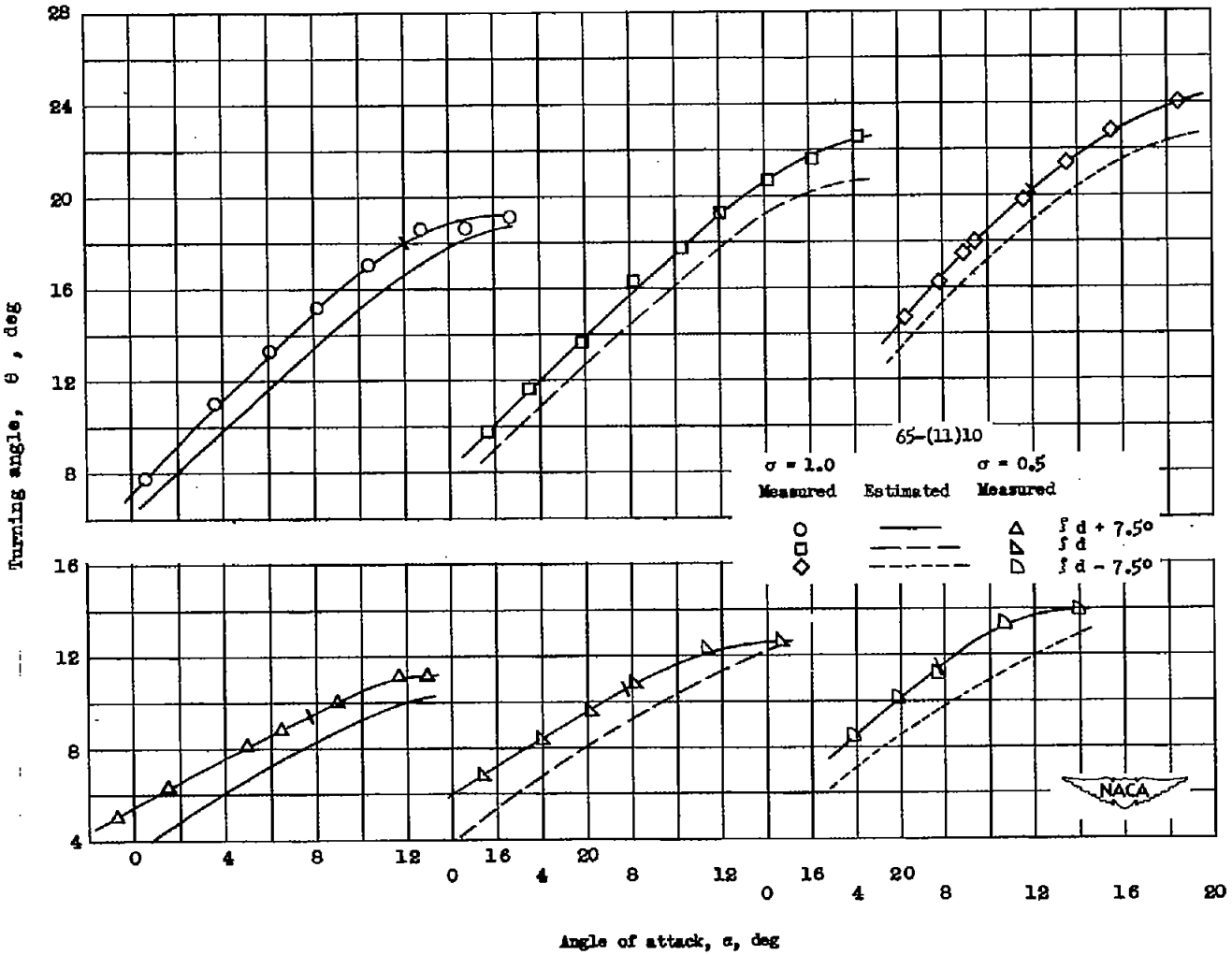

(b) Pitch section.

Figure 15.- Continued.

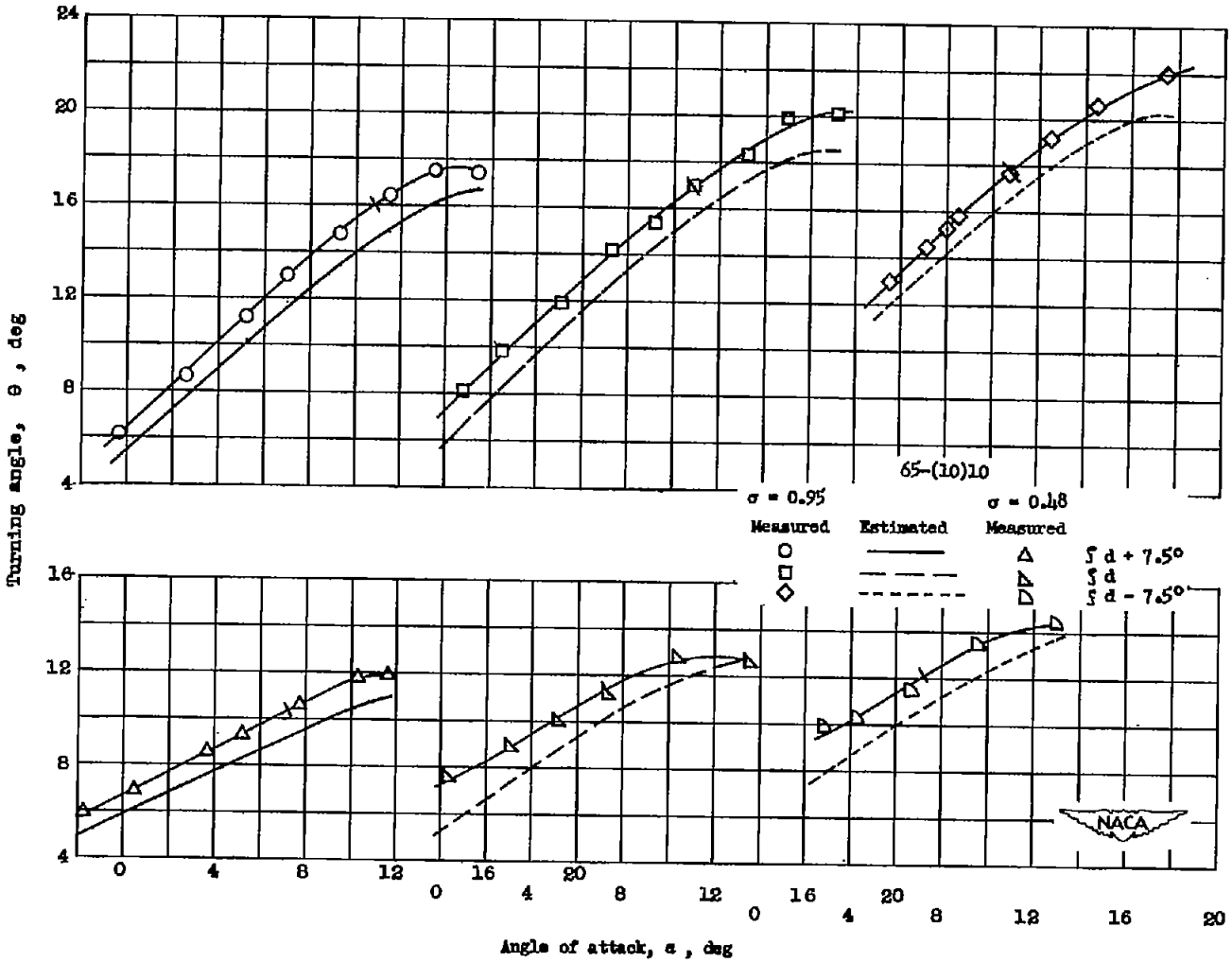

(c) Outboard section.

Figure 15.- Concluded.

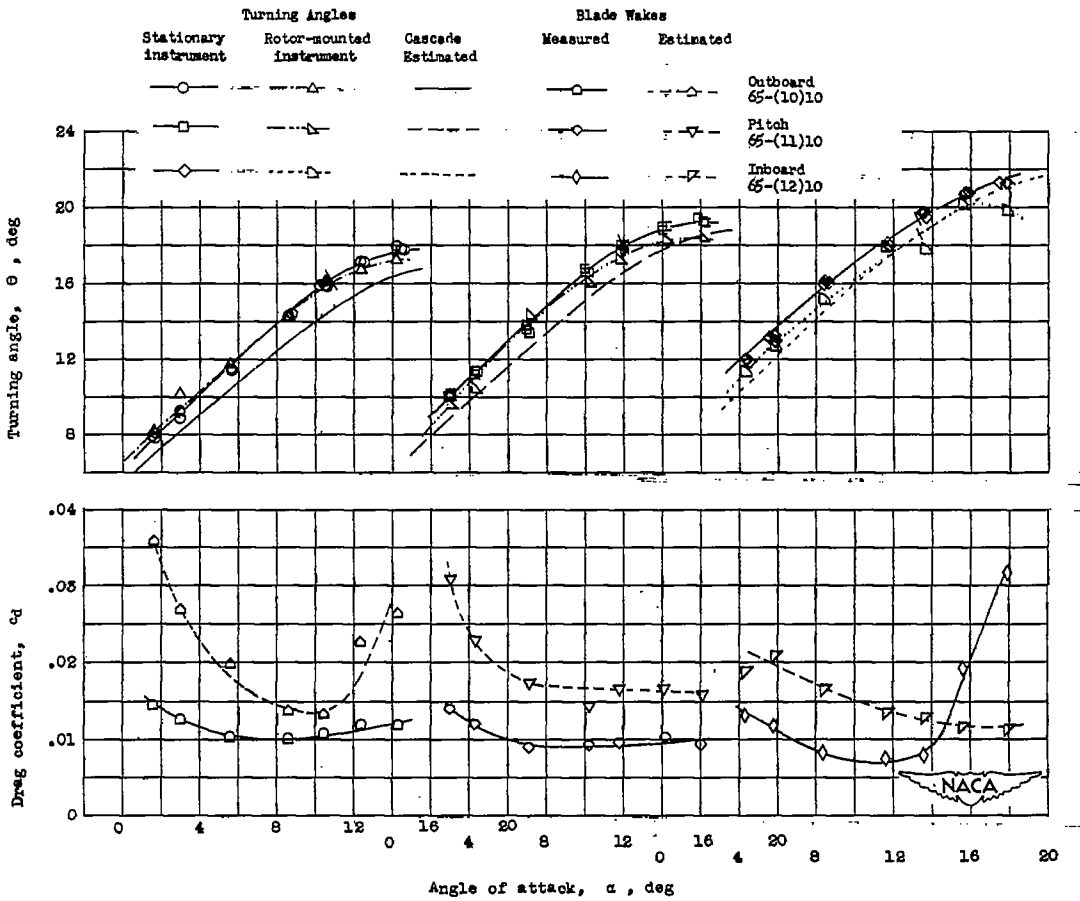

Figure 16.- Comparison of estimated variation of turning angle with angle of attack with measured values using stationary and rotor-mounted instruments, and comparison of measured and estimated wakes for the constant-annulus-area condition with a $7\frac{1}{2}^{\circ}$ above design blade angle at a solidity of 1.0. (Bars across curves indicate design point.)

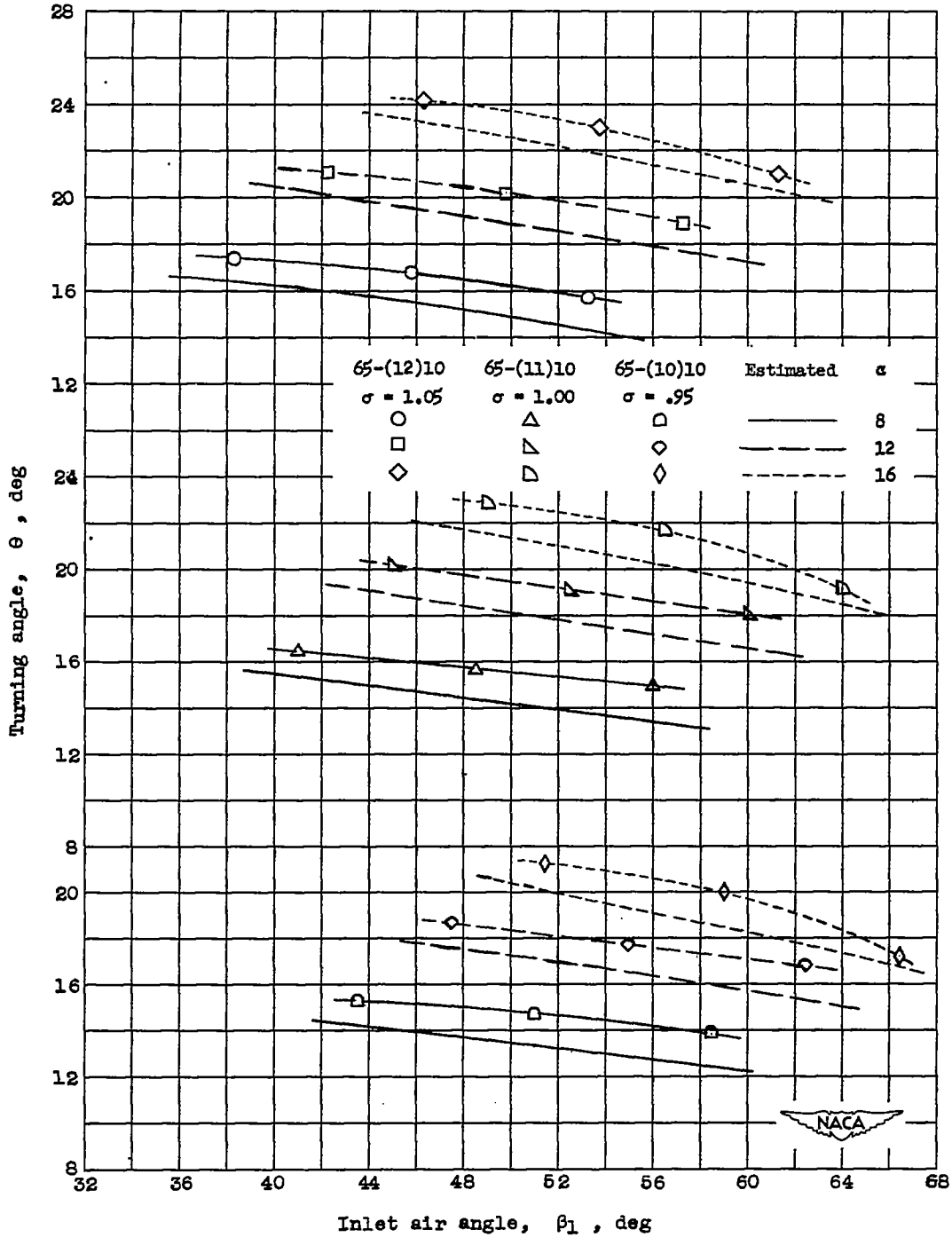

(a) Solidity of pitch section of 1.0.

Figure 17.- Variation of turning angle with inlet air angle at constant angles of attack as measured and estimated at the inboard, pitch, and outboard sections for constant-annulus-area tests at a solidity of 1.0.

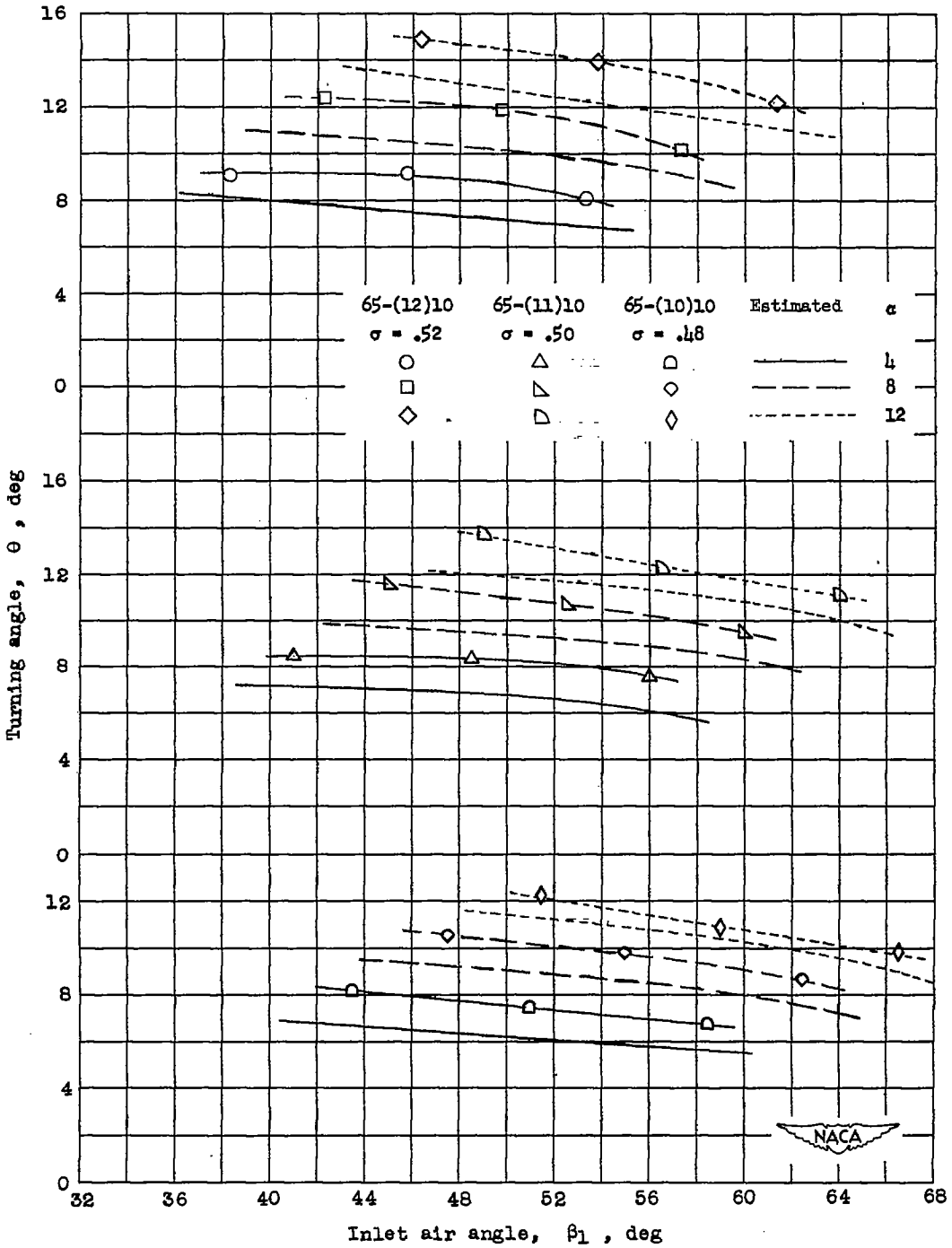

(b) Solidity of pitch section of 0.50.

Figure 17.- Concluded.

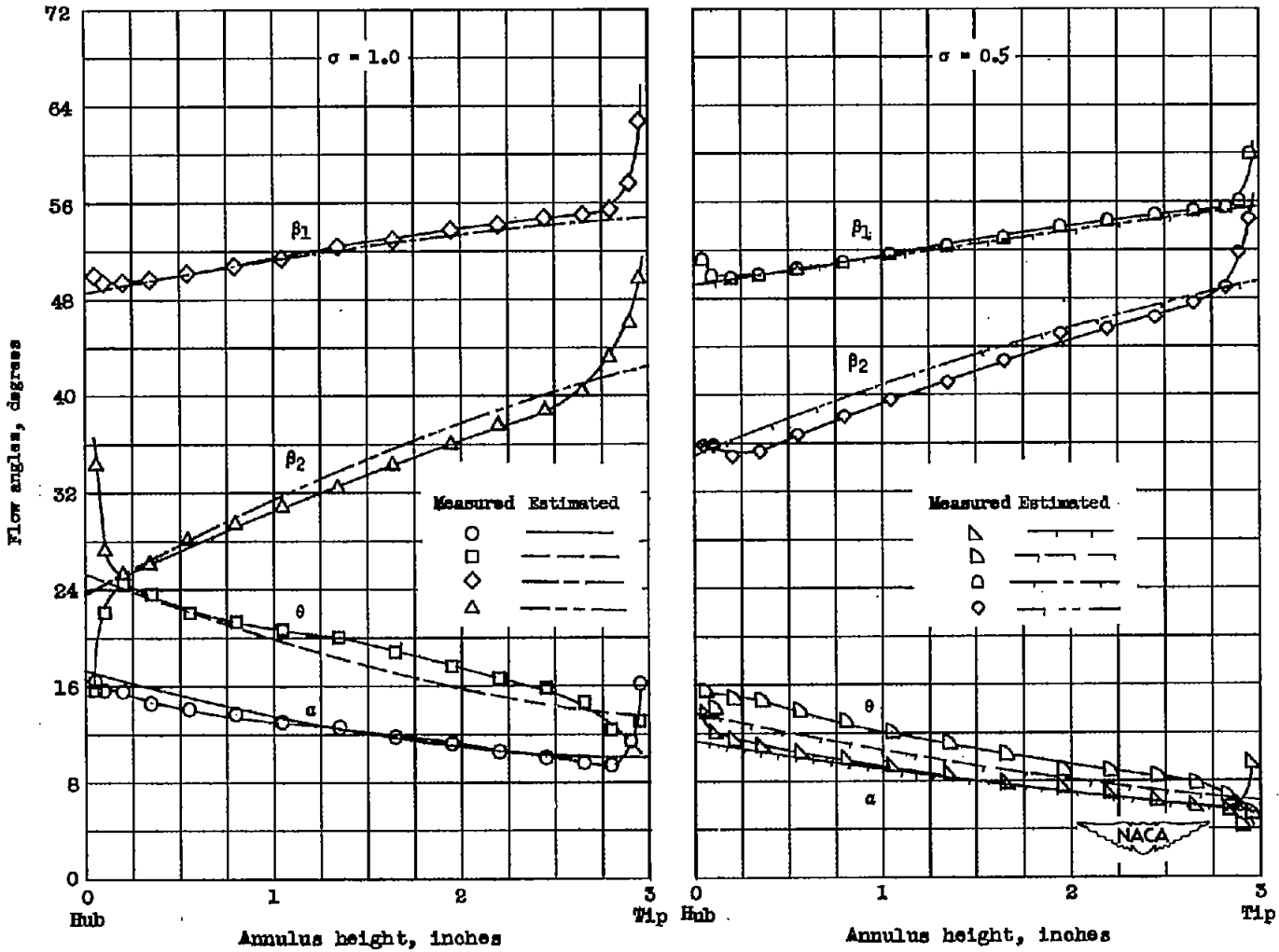

Figure 18.- Variation of measured and estimated flow angles relative to the rotor across the annulus for typical tests near design flow rate for design blade angle, constant annulus area, and solidities of 1.0 and 0.5.

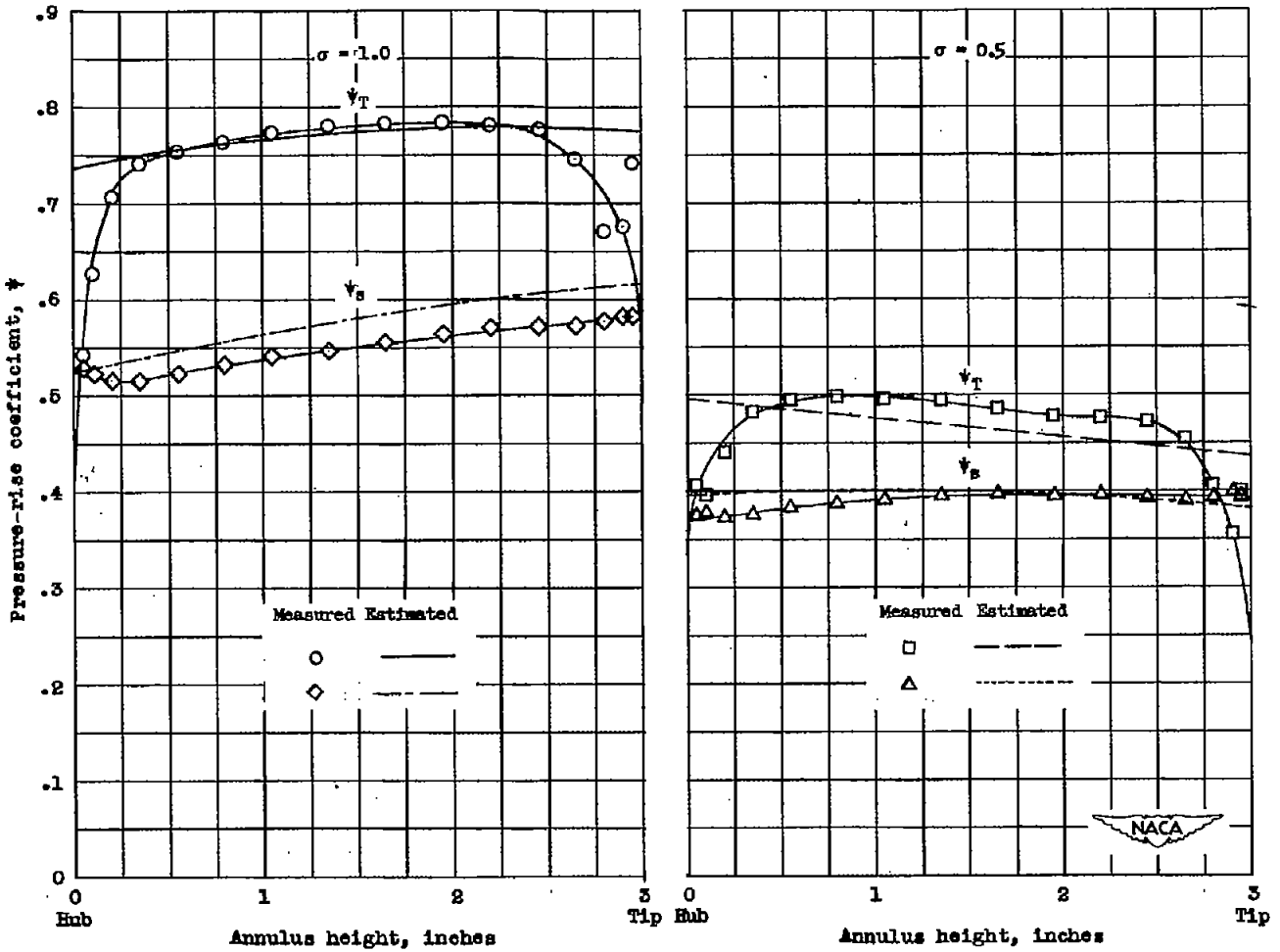

Figure 19.- Variation of measured and estimated total- and static-pressure-rise coefficients across the annulus for typical tests near design flow rate at the design blade angle, constant-annulus-area condition for solidities of 1.0 and 0.5.

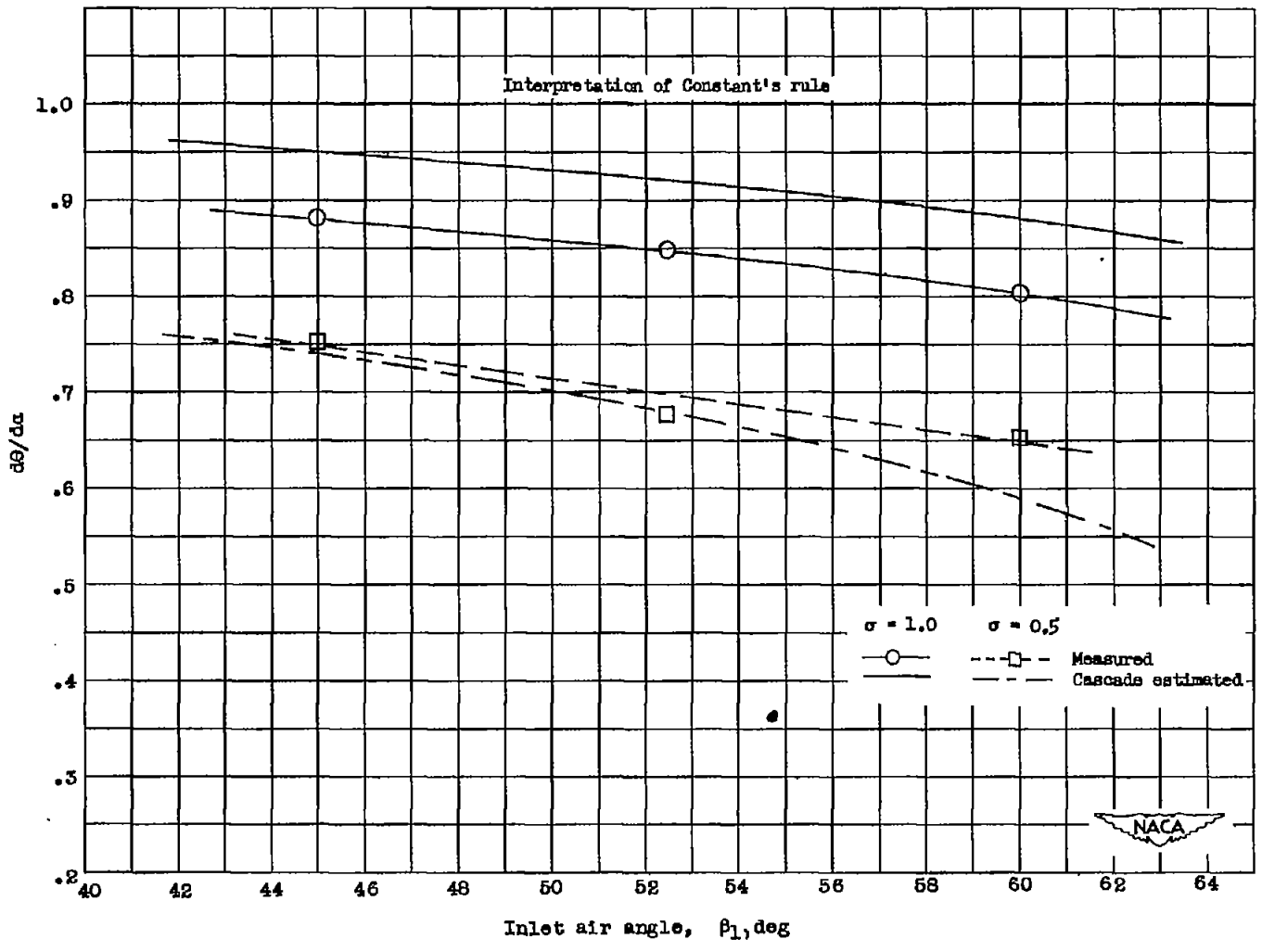

Figure 20.- Variation of average measured and estimated $d\theta/d\alpha$ values with inlet air angle for the constant-annulus-area tests at solidities of 1.0 and 0.5.

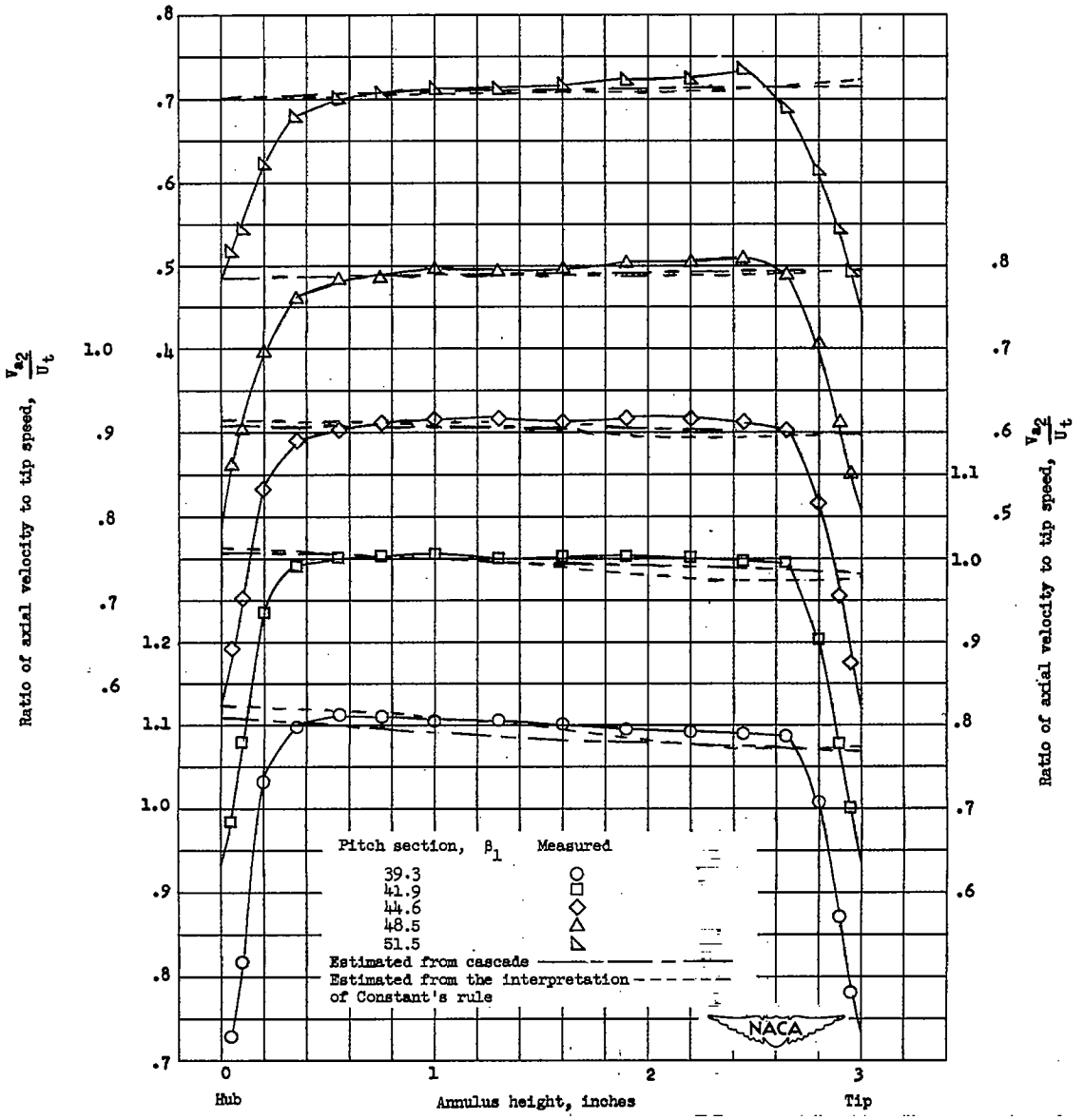

(a) $7\frac{1}{2}^{\circ}$ below design angle at a solidity of 1.0.

Figure 21.- Variation of measured and estimated axial velocities across the annulus in terms of U_t for five flow rates at the constant-annulus-area condition.

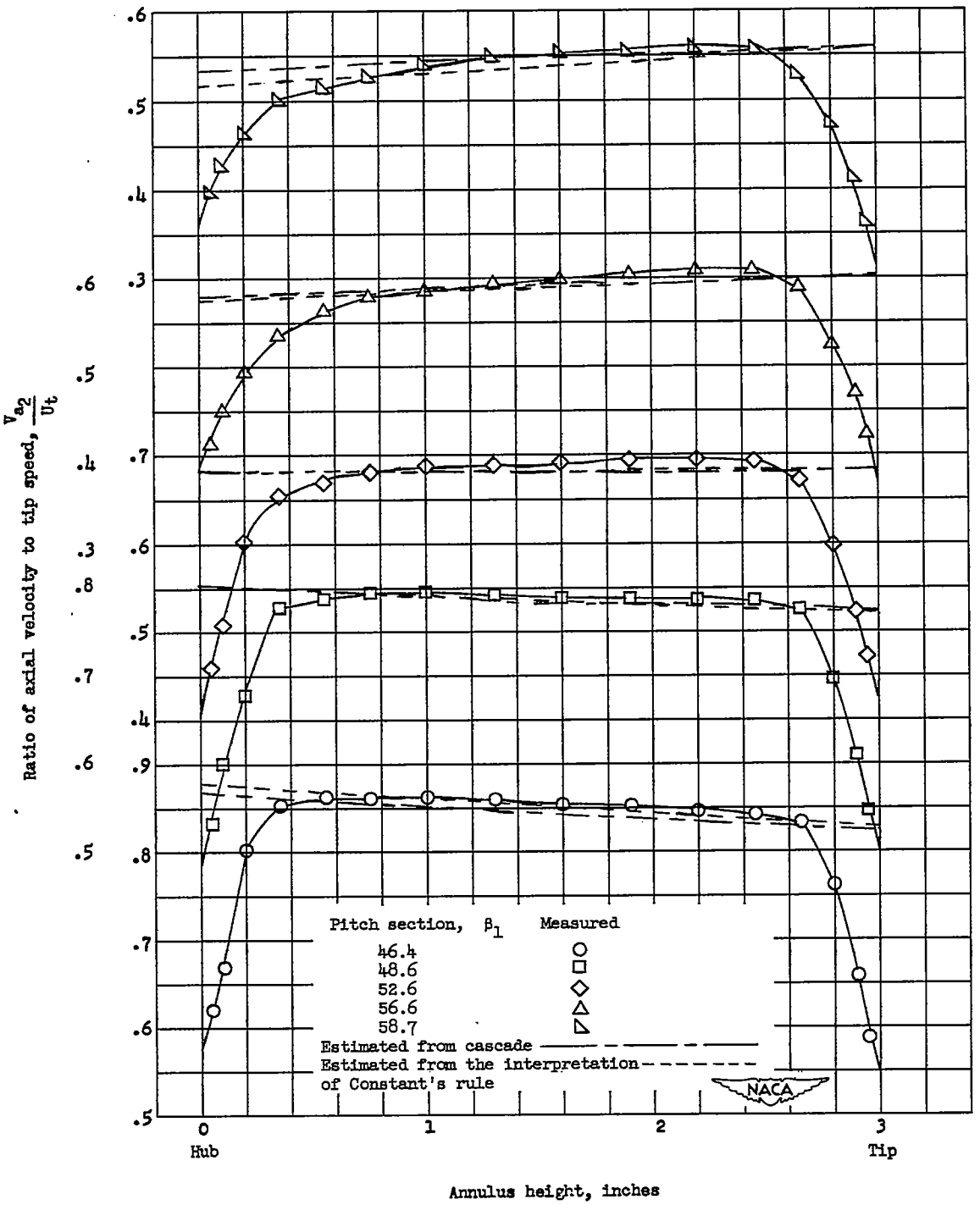

(b) Design blade angle at a solidity of 1.0.

Figure 21.- Continued.

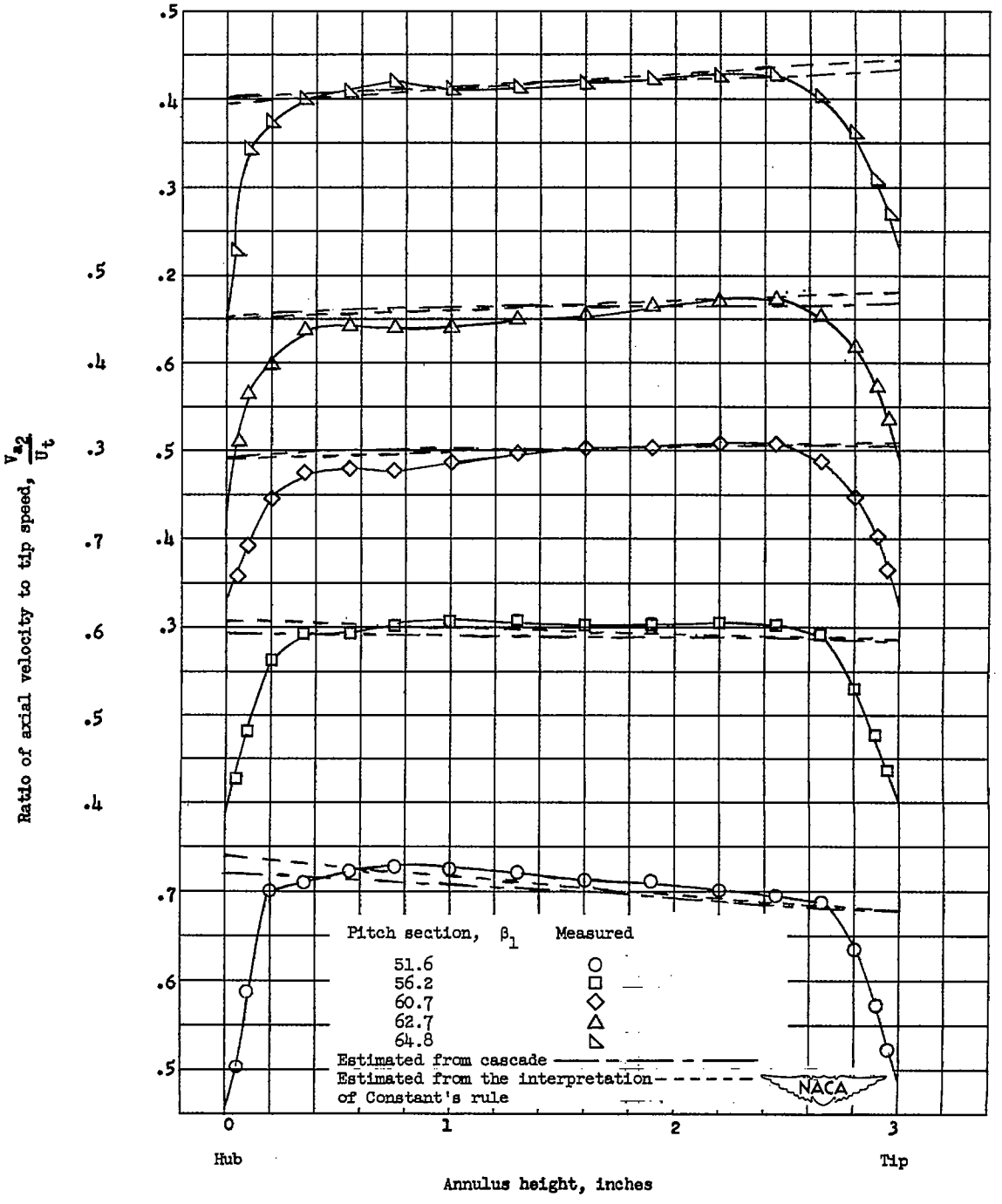

(c) $7\frac{1}{2}^{\circ}$ above design blade angle.

Figure 21.- Concluded.

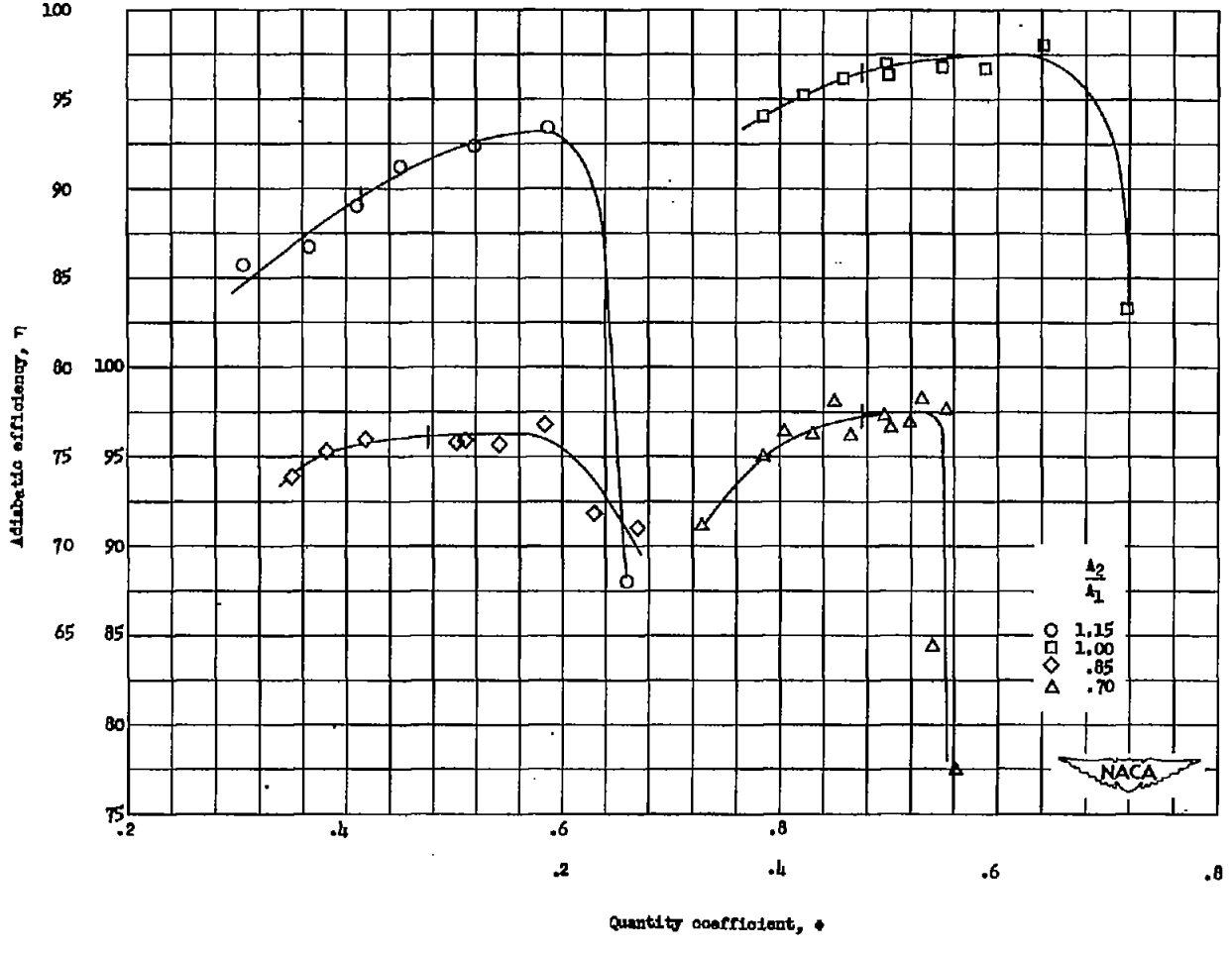

Figure 22.- Variation of adiabatic efficiency with quantity coefficient for $7\frac{1}{2}^{\circ}$ above design blade angle, solidity of 1.0, and annulus-area ratios of 1.15, 1.00, 0.85, and 0.70. (Vertical lines across curve indicate design points.)

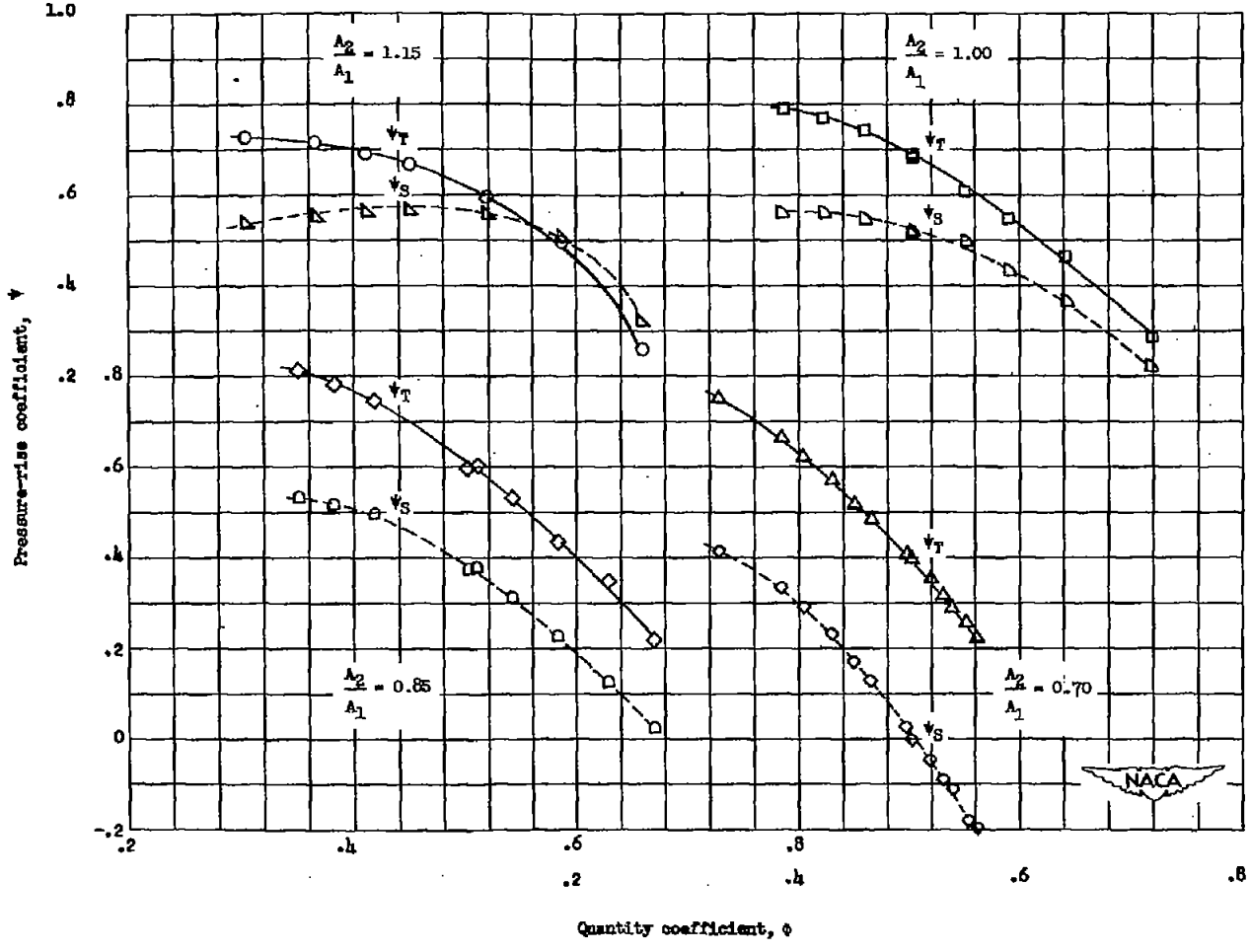

Figure 23.- Variation of total- and static-pressure-rise coefficients with quantity coefficient for $7\frac{1}{2}^\circ$ above design blade angle, solidity of 1.0, and annulus-area ratios of 1.15, 1.00, 0.85, and 0.70.

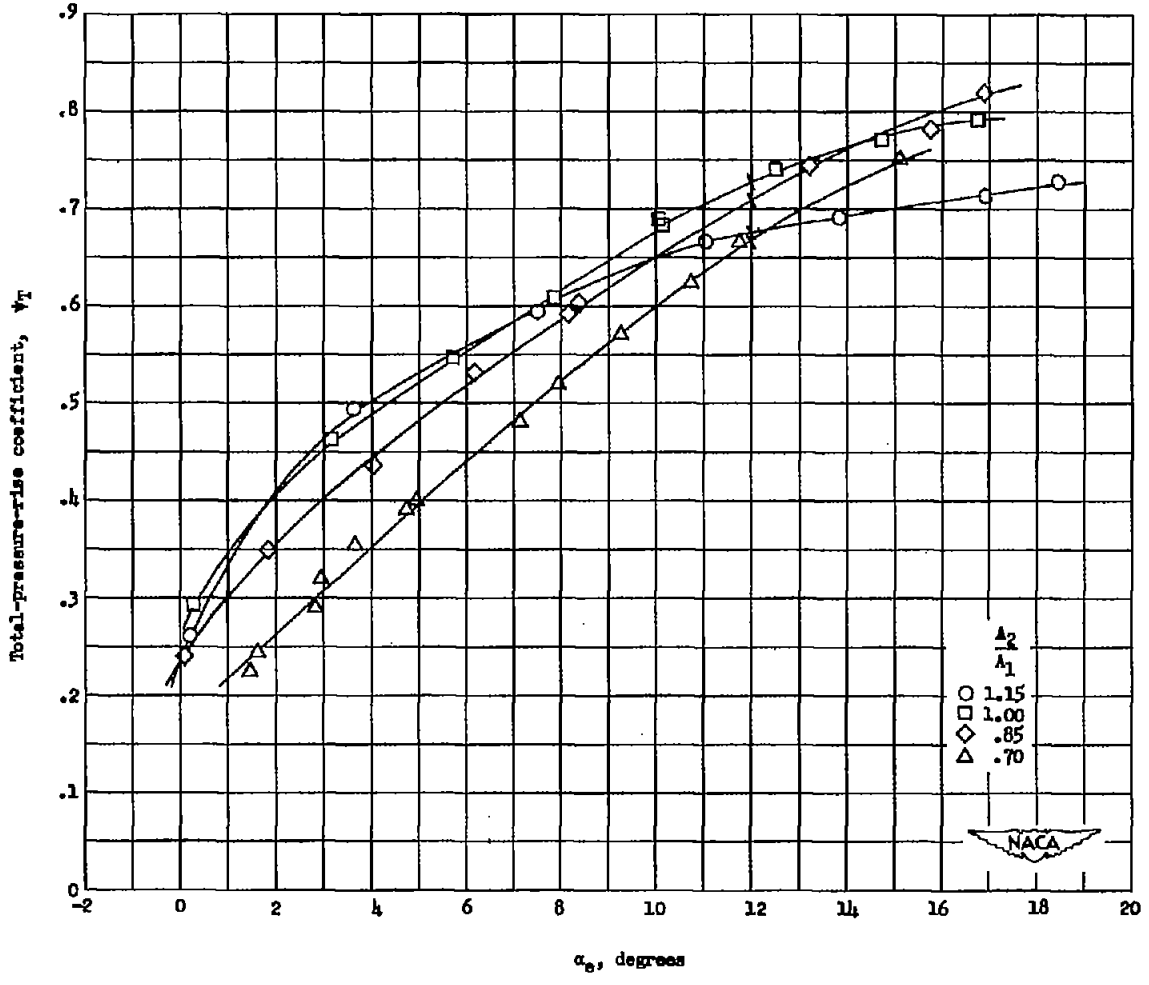

Figure 24.- Variation of total-pressure-rise coefficient ψ_T with effective angle of attack α_e at the pitch diameter for the several annulus-area ratios tested. (Bars across curves indicate design points.)

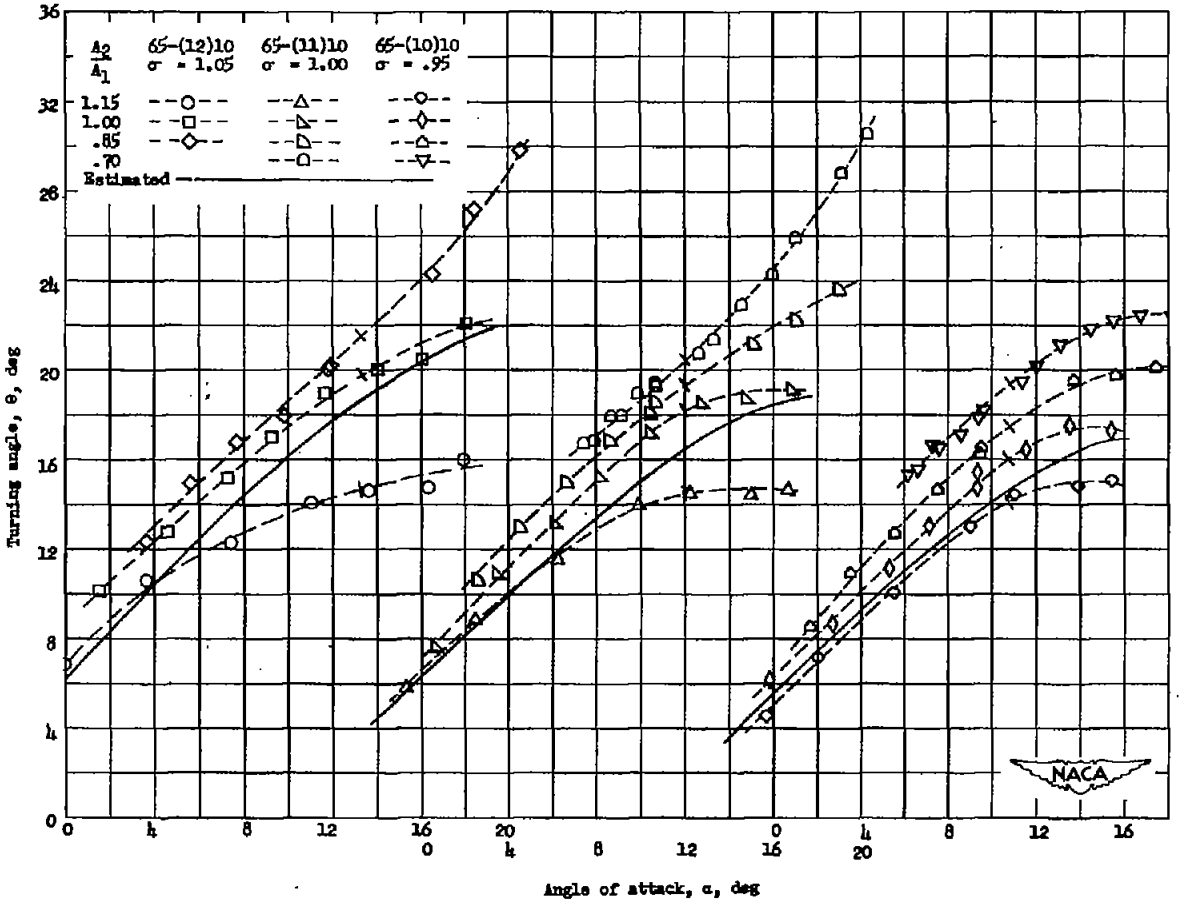

Figure 25.- Comparison of estimated and measured turning-angle variation with angle of attack at the inboard, pitch, and outboard blade sections for $7\frac{1}{2}^{\circ}$ above design blade angle, solidity of 1.0, and annulus-area ratios of 1.15, 1.00, 0.85, and 0.70. (Bars across curves indicate design points.)

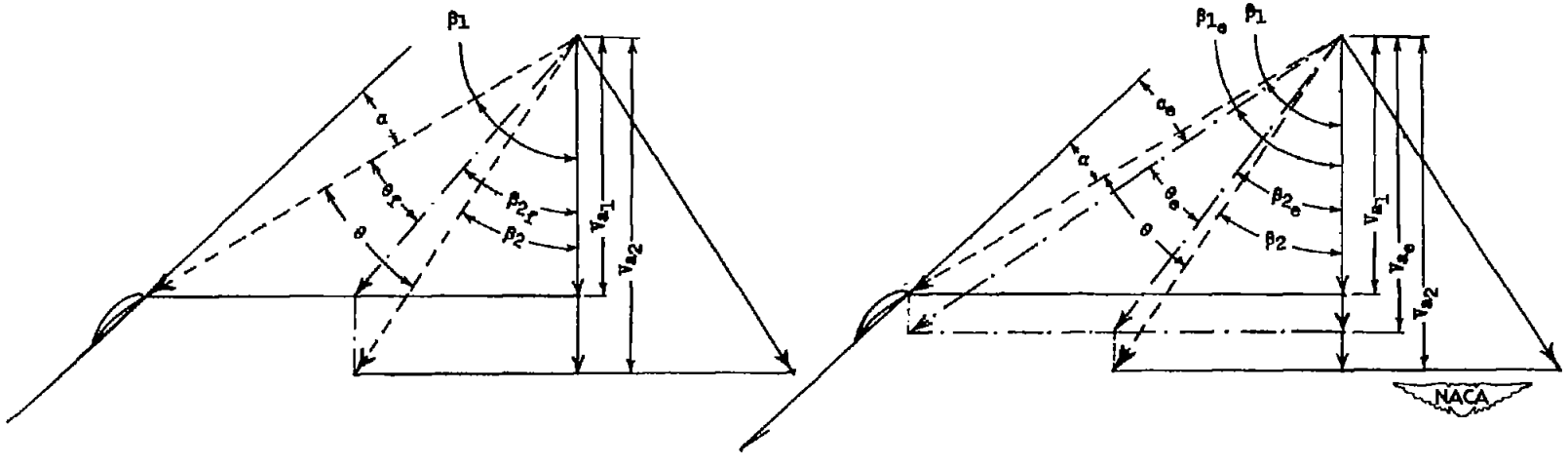

(a) Velocity vector diagram corrected to entering axial velocity.

(b) Velocity vector diagram corrected to mean axial velocity.

Figure 26.- Methods of correcting velocity vector diagrams of varying axial velocity to compare with constant-axial-velocity cascade or compressor results.

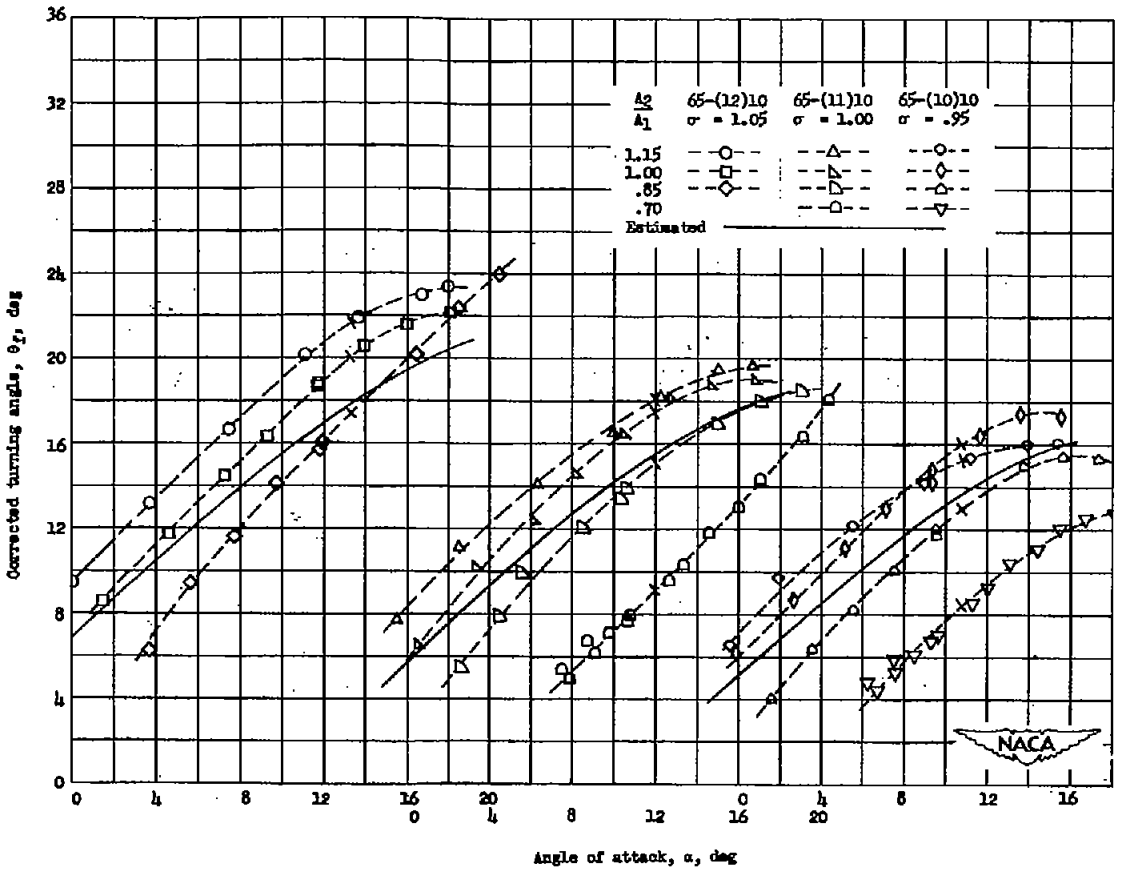

Figure 27.- Comparison of estimated and measured turning-angle variation with angle of attack at the inboard, pitch, and outboard blade sections for $7\frac{1}{2}^{\circ}$ above design blade angle, solidity of 1.0, and annulus-area ratios of 1.15, 1.00, 0.85, and 0.70 using the constant-circulation system corrected to the entering axial velocity. (Bars across curves indicate design points.)

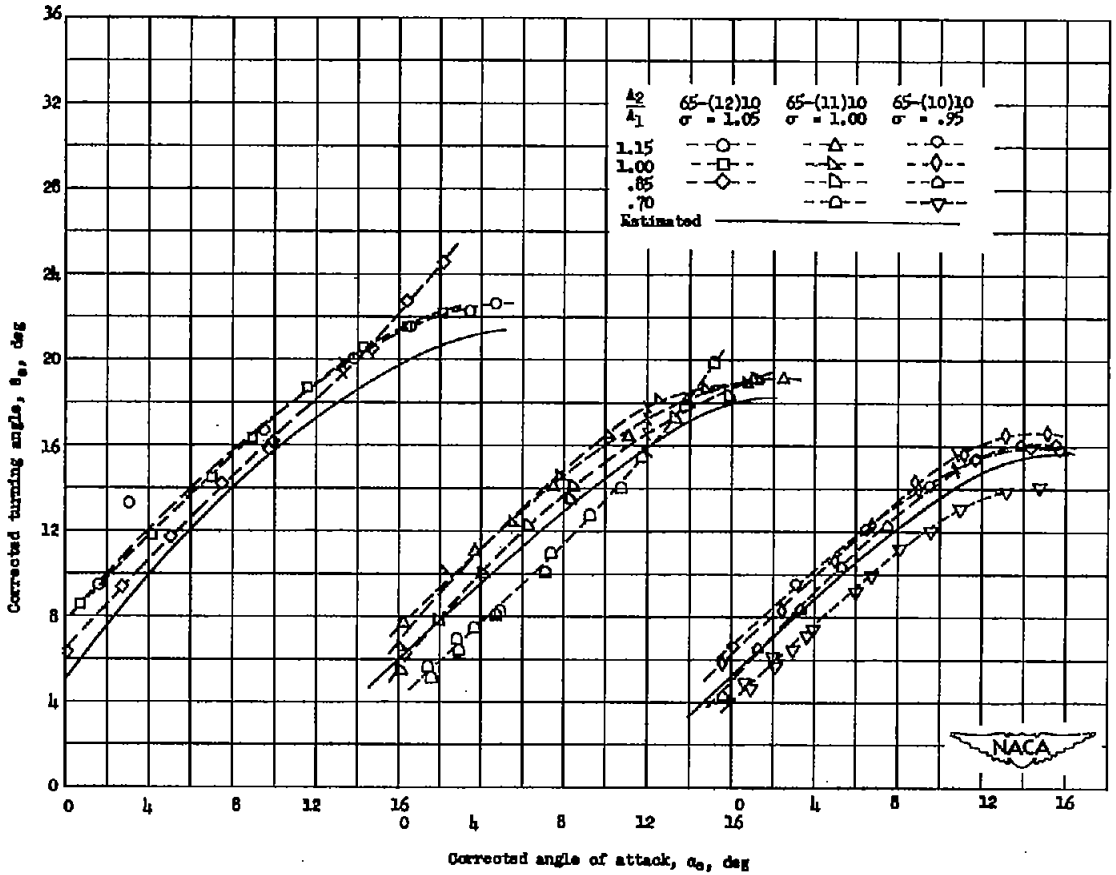

Figure 28.- Comparison of estimated and measured turning-angle variation with angle of attack at the inboard, pitch, and outboard blade sections for $7\frac{1}{2}^{\circ}$ above design blade angle, solidity of 1.0, and annulus-area ratios of 1.15, 1.00, 0.85, and 0.70 using the constant-circulation system corrected to the mean axial velocities. (Bars across curves indicate design points.)

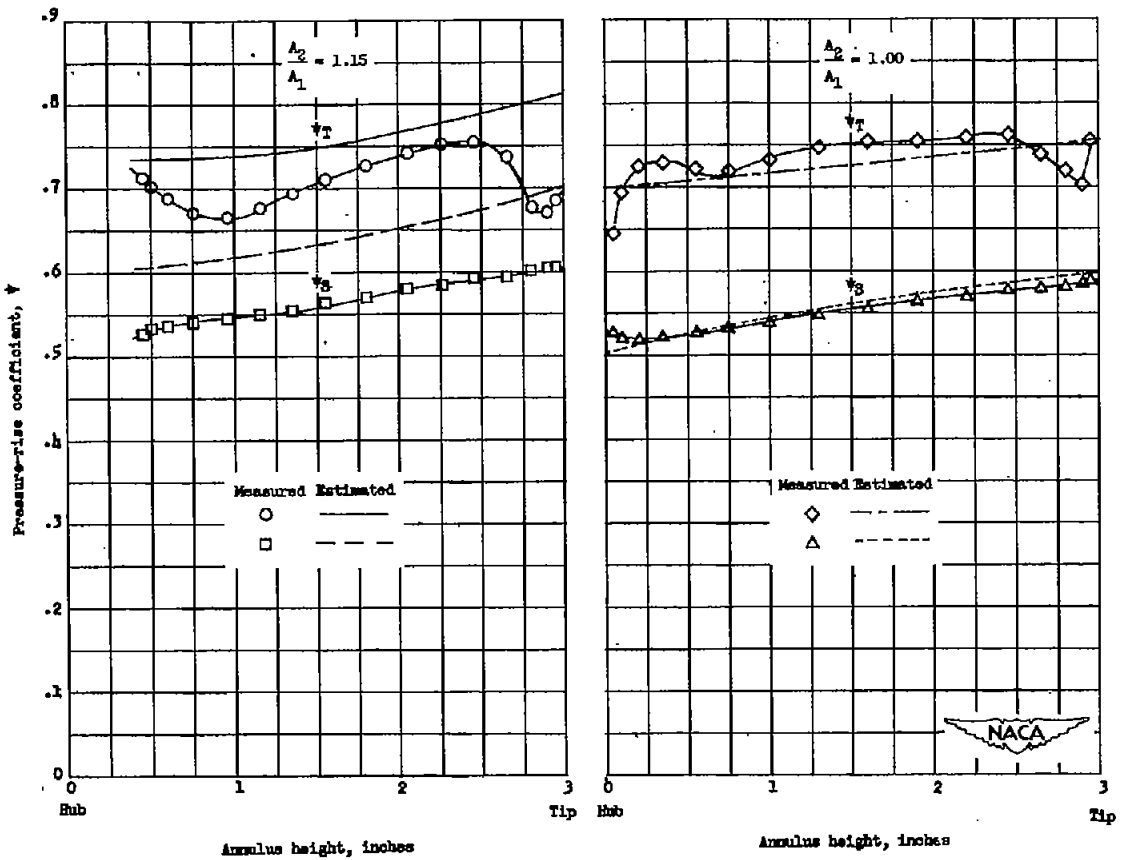

(a) Annulus-area ratios of 1.15 and 1.00.

Figure 29.- Variation of measured total- and static-pressure-rise coefficients across the annulus as compared with values estimated using the mean-axial-velocity, constant-circulation system for $7\frac{1}{2}^\circ$ above design blade angle, and solidity of 1.0.

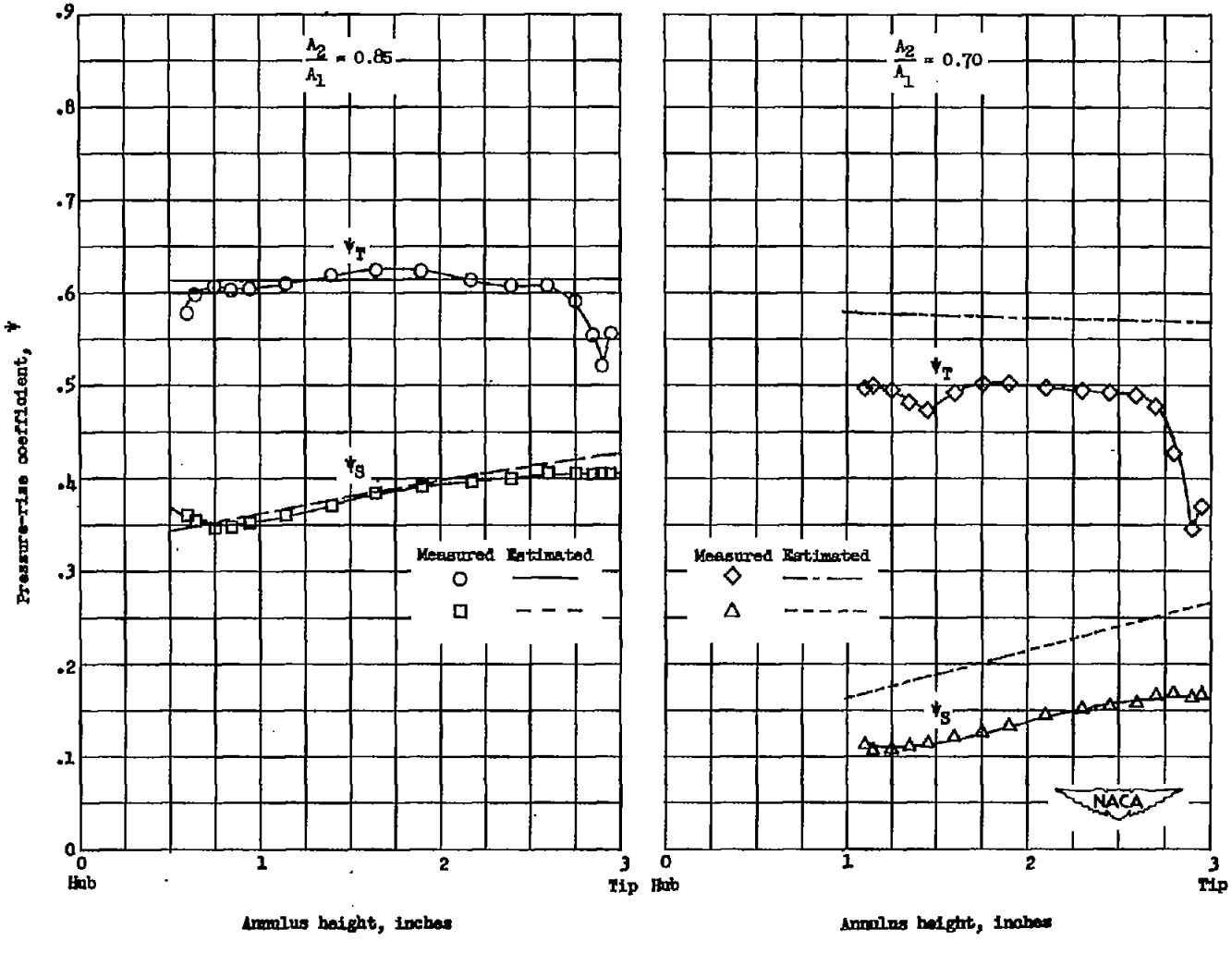

(b) Annulus-area ratios of 0.85 and 0.70.

Figure 29.- Concluded.

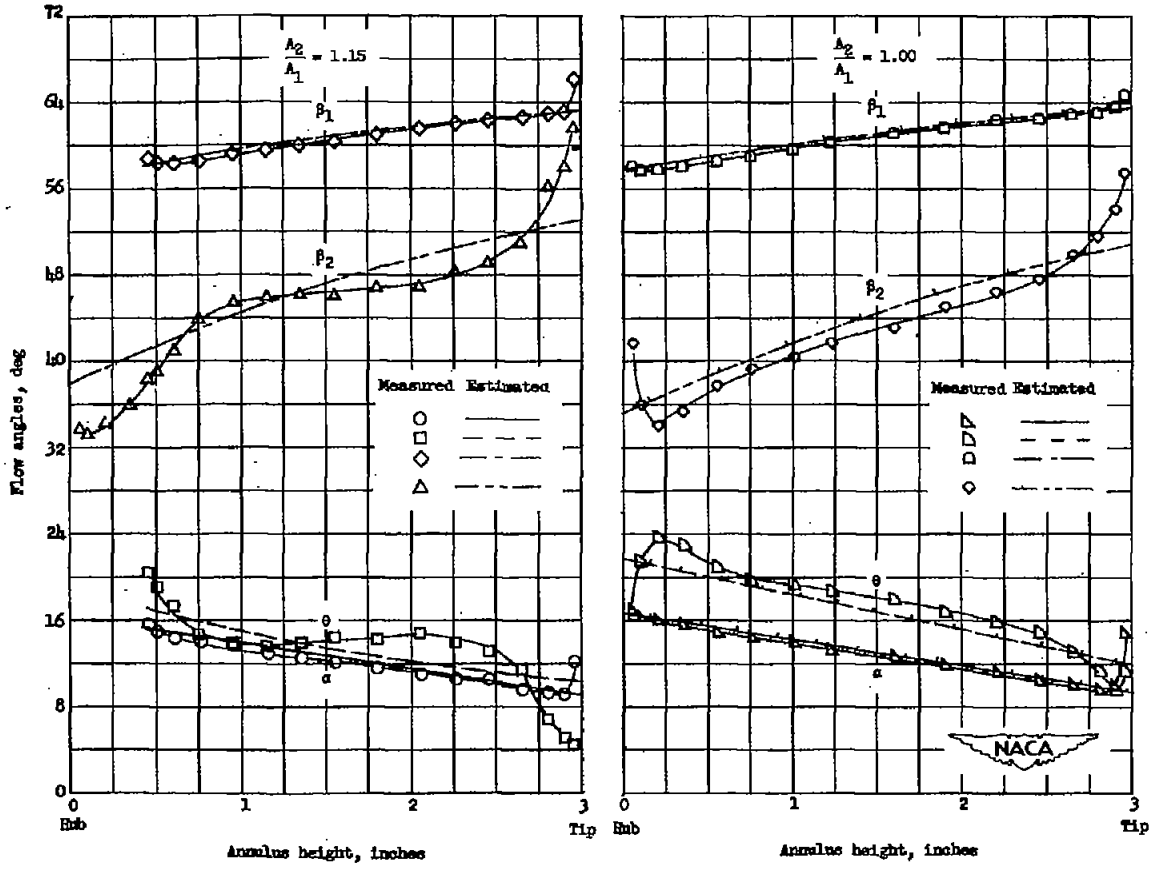

(a) Annulus-area ratios of 1.15 and 1.00.

Figure 30.- Variation of measured flow angles relative to the rotor across the annulus as compared with values estimated using the mean-axial-velocity, constant-circulation system for $7\frac{1}{2}^{\circ}$ above design blade angle, and solidity of 1.0.

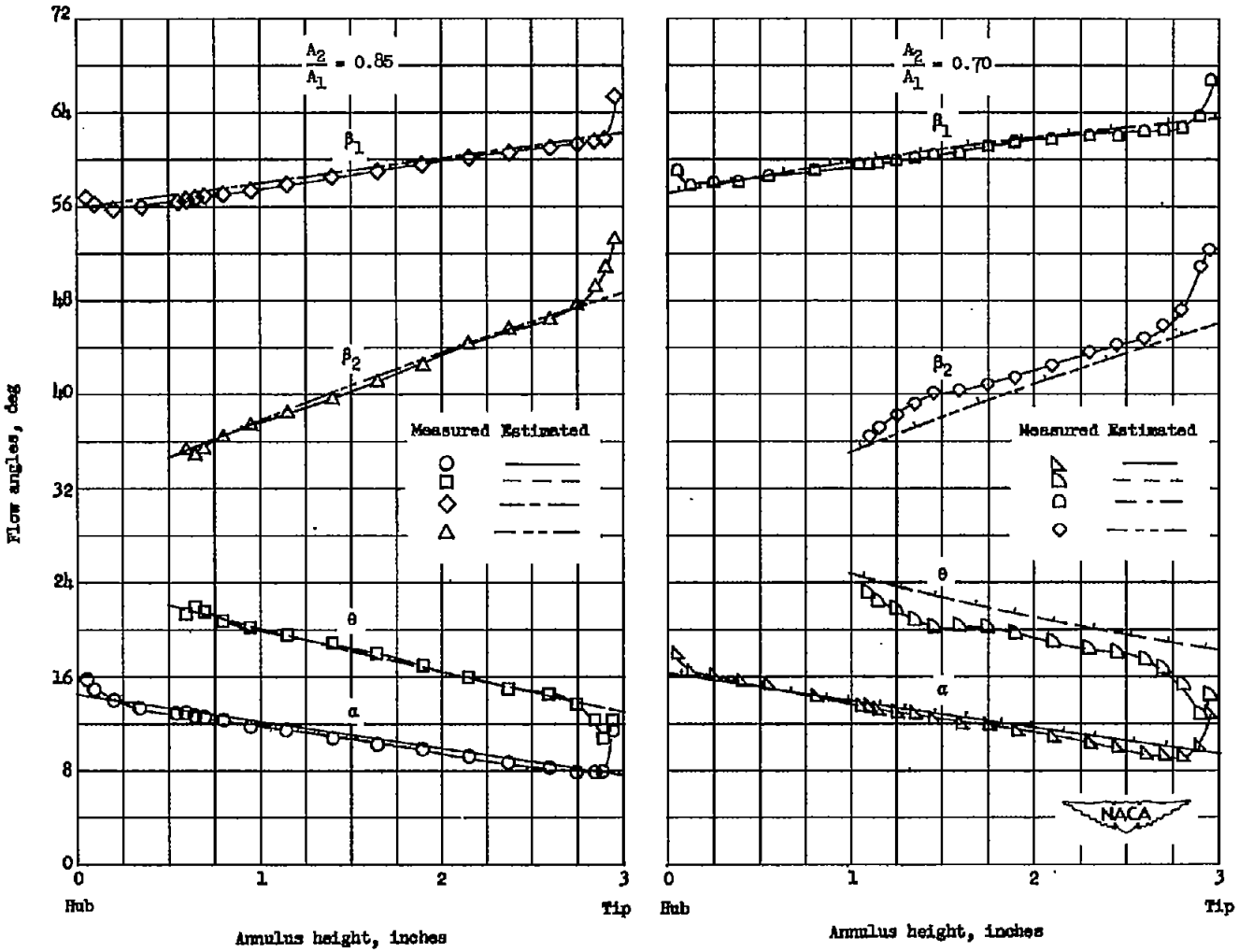

(b) Annulus-area ratios of 0.85 and 0.70.

Figure 30.- Concluded.

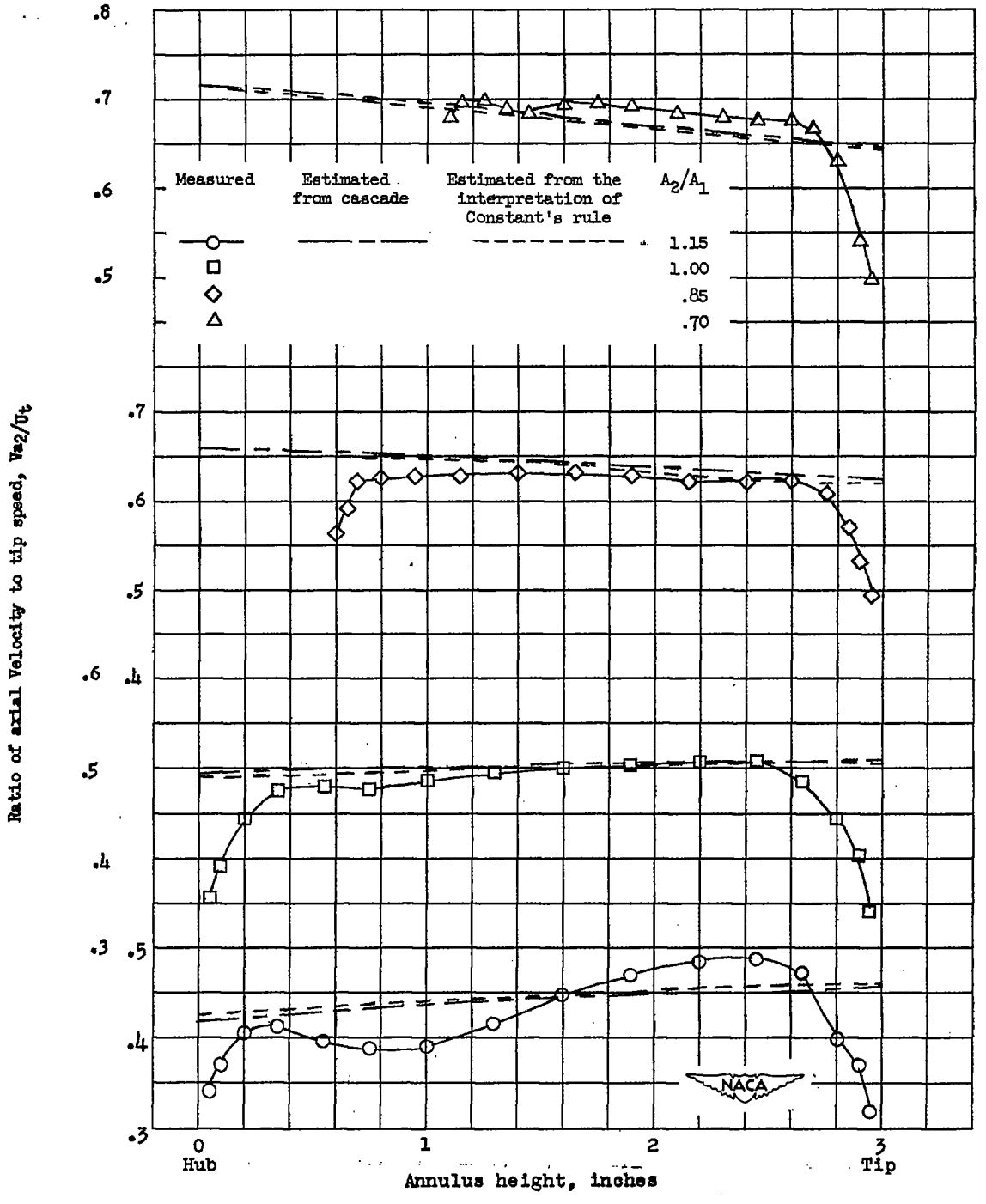

Figure 31.- Variation of measured and estimated axial velocities across the annulus in terms of U_t at flow rates near design for $7\frac{1}{2}^\circ$ above design blade angle, solidity of 1.0, and annulus-area ratios of 1.15, 1.00, 0.85, and 0.70.

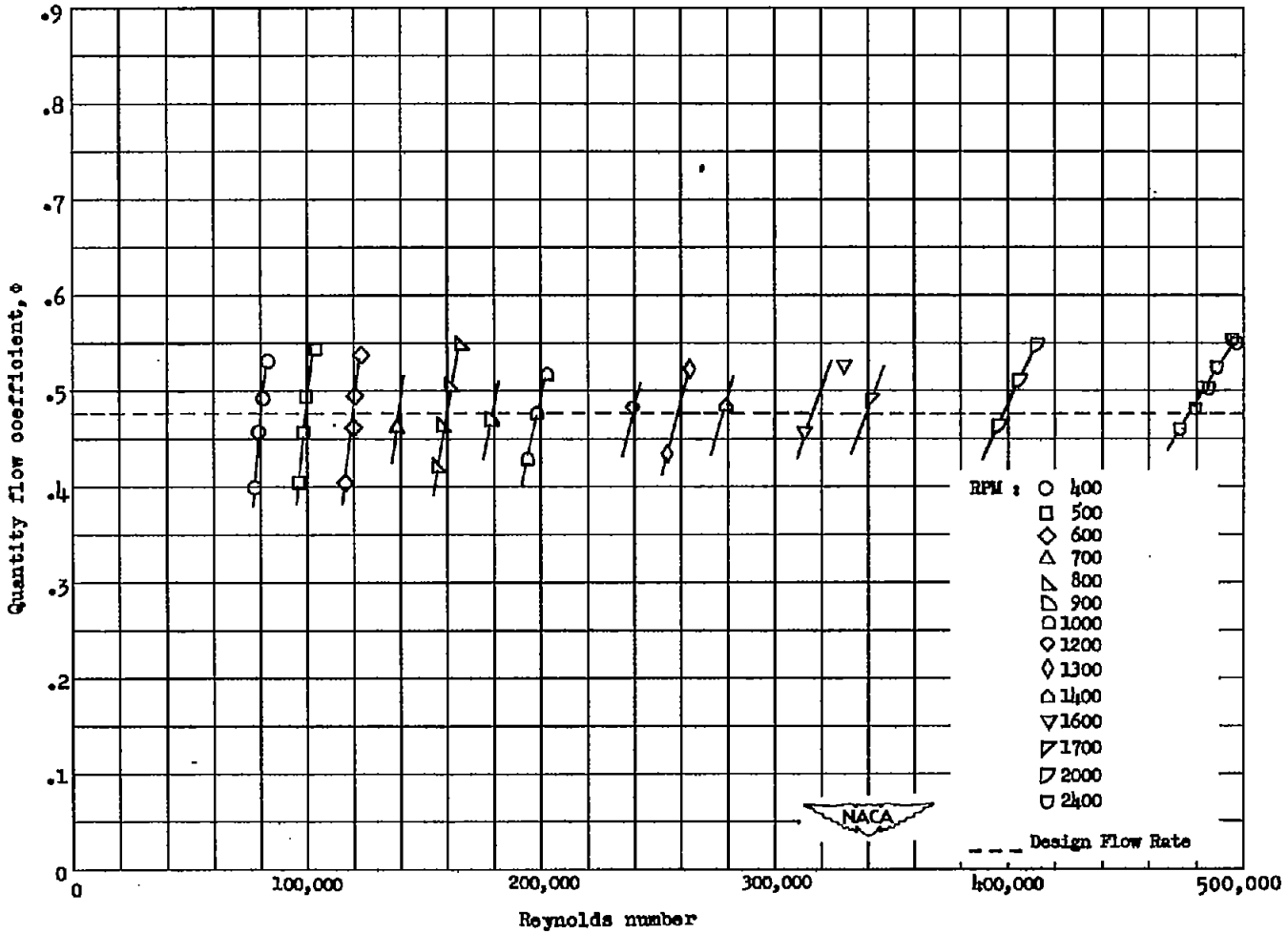

Figure 32.- Relation of Reynolds number effect test points with the design quantity flow coefficient at solidity of 1.0, $7\frac{1}{2}^{\circ}$ above design blade angle, and constant annulus area.

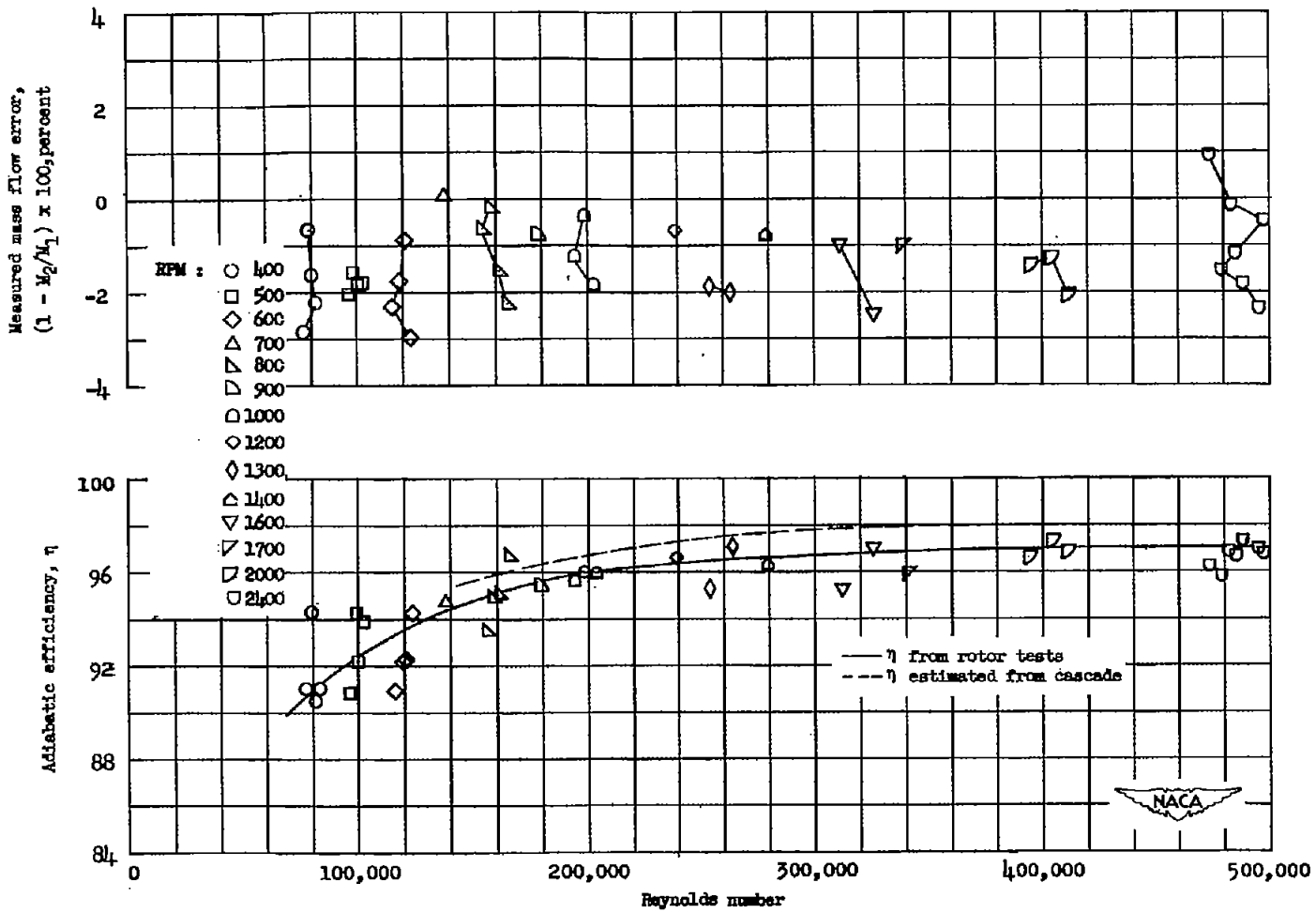

Figure 33.- Variation of measured mass flow error and measured and estimated efficiencies with Reynolds number at solidity of 1.0, $7\frac{1}{2}^{\circ}$ above design blade angle, and constant annulus area.

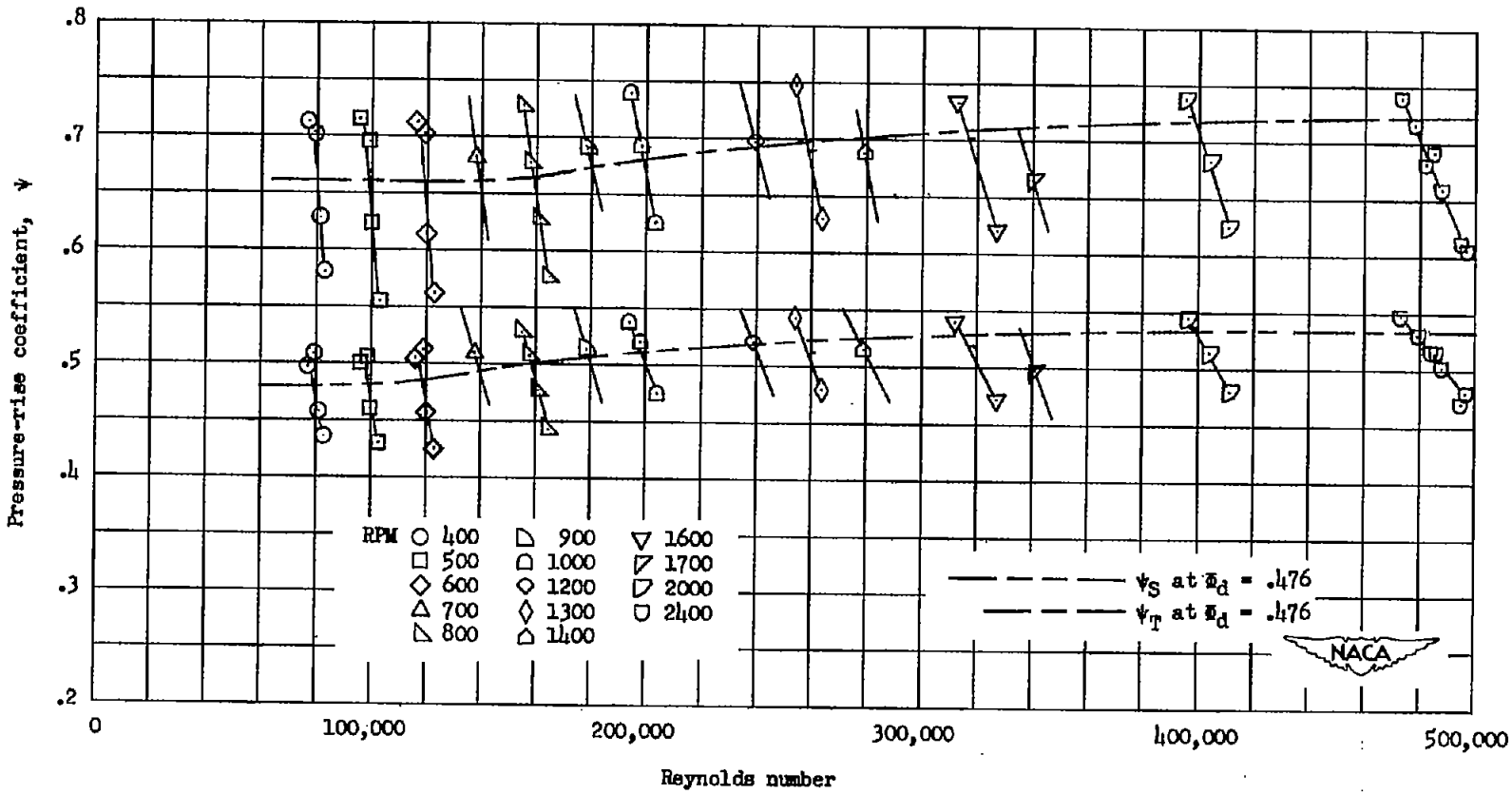

Figure 34.- Variation of static- and total-pressure-rise coefficient with Reynolds number at a solidity of 1.0, $7\frac{1}{2}^{\circ}$ above design blade angle, and constant annulus area.

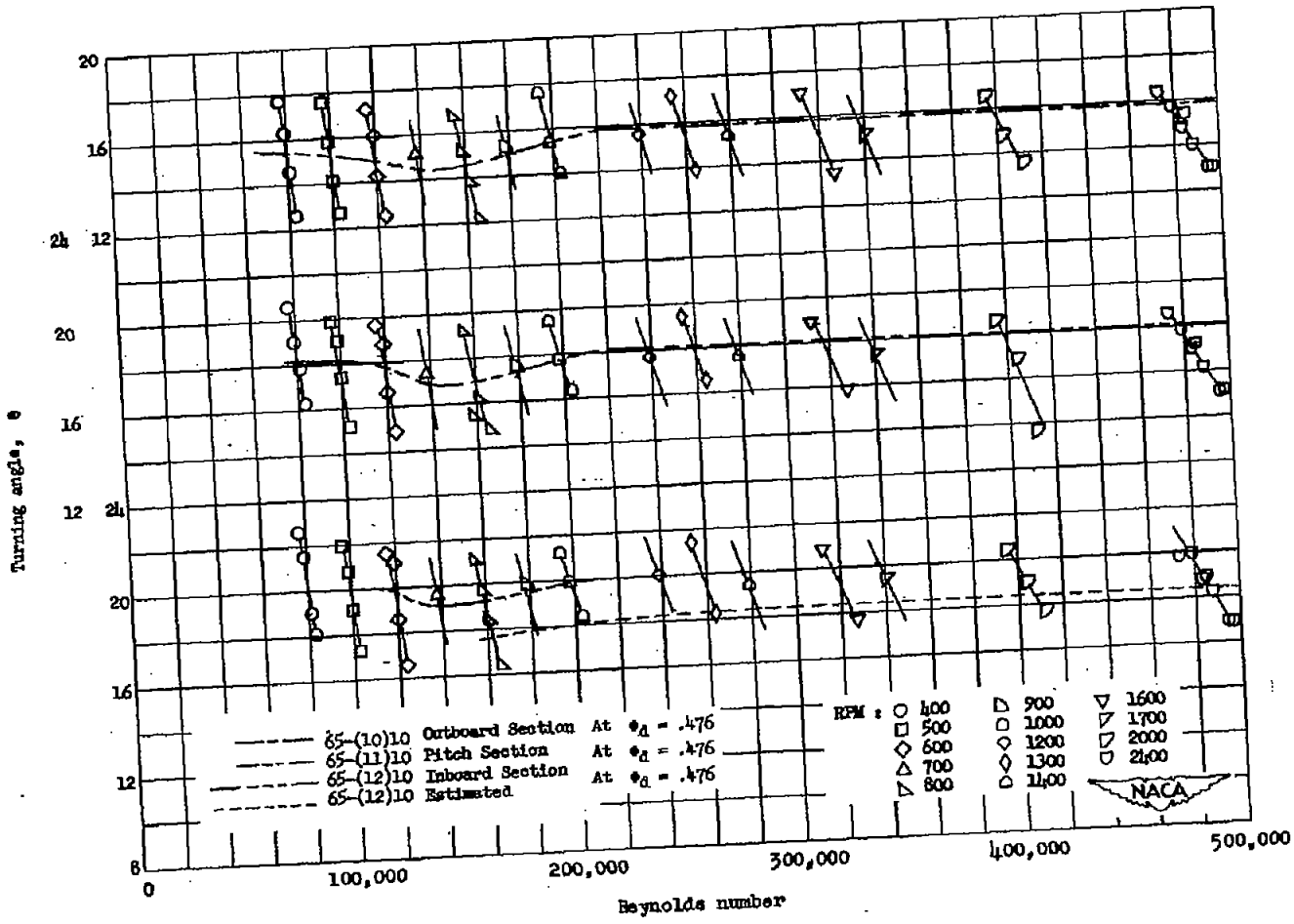

Figure 35.- Variation of measured and cascade estimated turning angles with Reynolds number at the inboard, pitch, and outboard sections for a solidity of 1.0, $7\frac{1}{2}^{\circ}$ above design blade angle, and constant annulus area.

NACA - Langley Field, Va.